Chinese Chemical Letters 37 (2026) 112179

Contents lists available at ScienceDirect

Chinese Chemical Letters

journal homepage: www.elsevier.com/locate/cclet

Structure–function correlation and design principles of two-dimensional bismuth nanosheets for efficient electrochemical CO_2 reduction

Chuncheng Xu[a], Suqin Han[a], Kaiyang Zhang[a], Qiuling Feng[a], Lan Bao[a], Mingming Gao[a], Wen-Yan Gao[c], Yen Leng Pak[a], Hongyu Mou[a], Liwei Chen[a,*], Xing Gao[a,*], Yuchen Hao[b,*]

[a] College of Biological and Chemical Engineering, Qilu Institute of Technology, Ji'nan 250200, China
[b] Research Center for Solar Driven Carbon Neutrality, School of Physics Science and Technology, Institute of Life Science and Green Development, Hebei University, Baoding 071002, China
[c] Luoyang Center for Teacher Development, Luoyang 471000, China

ARTICLE INFO

Article history:
Received 16 September 2025
Revised 21 November 2025
Accepted 26 November 2025
Available online 27 November 2025

Keywords:
Two-dimensional materials
Bismuth nanosheets
Synthesis strategies
Electrocatalysis
CO_2 reduction

ABSTRACT

Electrochemical reduction of carbon dioxide (CO_2RR) into formate and related products is a crucial strategy for sustainable carbon utilization, yet the development of catalysts with both high efficiency and durability remains a central challenge. Among available candidates, two-dimensional (2D) bismuth (Bi) nanosheets stand out because of their earth abundance, low toxicity, and unique ability to stabilize *OCHO intermediates. In this review, we systematically summarize recent advances in the controlled synthesis of 2D Bi nanosheets, covering bottom-up chemical and electrochemical routes, top-down exfoliation, and physical/thermal methods, and highlight the application strategies that enable performance optimization, including defect/strain engineering, heteroatom doping, interface construction, heterostructure coupling, *in situ* reconstruction, and microenvironment regulation. We further integrate mechanistic insights from *in situ/operando* characterizations and density functional theory, which clarify the real active sites, dynamic reconstruction, and structure–activity relationships. Finally, we provide a forward-looking perspective on atomic-level structural control, understanding and regulating reconstruction, multi-scale architecture integration, expanding product selectivity beyond formate, device-level optimization, and data-driven catalyst discovery. By bridging synthesis, application strategies, and mechanistic understanding, this timely review establishes a comprehensive framework to guide the rational design of 2D Bi nanosheets and accelerate their translation toward industrially relevant CO_2 electroreduction.

© 2025 Published by Elsevier B.V. on behalf of Chinese Chemical Society and Institute of Materia Medica, Chinese Academy of Medical Sciences.

1. Introduction

The accelerating consumption of fossil fuels and the accompanying surge in anthropogenic CO_2 emissions have brought about severe environmental challenges, including climate change and energy insecurity [1–5]. In this context, the electrochemical CO_2 reduction reaction (CO_2RR), driven by renewable electricity, has emerged as a promising strategy to simultaneously alleviate atmospheric CO_2 accumulation and produce value-added carbon-based fuels and chemicals [6,7]. Among the possible CO_2RR products, formic acid/formate ($HCOOH/HCOO^-$) has attracted particular interest due to its high volumetric energy density, wide applications in fuel cells and chemical synthesis, and convenient storage and transportation [8–11]. However, realizing efficient, selective, and durable electrochemical conversion of CO_2 to formate under industrially relevant conditions remains highly challenging, and the development of advanced catalysts is of paramount importance [12].

Two-dimensional (2D) materials provide unique opportunities for CO_2RR catalysis owing to their high surface-to-volume ratio, tunable surface chemistry, and abundant low-coordination active sites [13–15]. Within this family, 2D bismuth nanosheets (Bi NSs) have garnered significant attention as ideal CO_2RR electrocatalysts [16,17]. Bismuth is earth-abundant, environmentally benign, and exhibits intrinsically favorable binding to the key *OCHO intermediate, thereby ensuring excellent selectivity for formate formation [18,19]. Moreover, the electronic structure of 2D Bi NSs can be readily modulated through defect engineering, doping, interface construction, and external strain, enabling tailored catalytic perfor-

* Corresponding authors.
E-mail addresses: chenliwei@qlit.edu.cn (L. Chen), gaoxing620@126.com (X. Gao), haoyc@hbu.edu.cn (Y. Hao).

https://doi.org/10.1016/j.cclet.2025.112179
1001-8417/© 2025 Published by Elsevier B.V. on behalf of Chinese Chemical Society and Institute of Materia Medica, Chinese Academy of Medical Sciences.

mance [20–23]. These advantages render Bi NSs one of the most promising platforms for CO_2-to-formate conversion [24–27].

Despite rapid progress, the controlled synthesis and mechanistic understanding of 2D Bi NSs remain in their infancy [28,29]. First, the intrinsic anisotropy and high surface energy of Bi make it difficult to achieve controlled bottom-up growth or top-down exfoliation, often resulting in limited lateral dimensions, poor crystallinity, or uncontrolled thickness [30–32]. Furthermore, advanced vapor-phase and epitaxial strategies, though promising, still face challenges in scalability and structural stability [33–36]. Second, although numerous strategies—such as defect creation, strain engineering, heterostructure integration, and dynamic reconstruction—have been explored to enhance CO_2RR activity, the precise correlation between structural motifs, electronic modulation, and catalytic performance is far from fully understood [37,38]. In particular, the dynamic structural evolution of Bi-based catalysts under electrochemical conditions complicates the identification of true active sites, limiting rational design [39–43].

Although several reviews have summarized the broader aspects of bismuth-based materials for CO_2RR, a systematic and in-depth discussion dedicated to two-dimensional Bi NSs, encompassing their synthesis challenges, controlled preparation strategies, and catalytic applications, remains absent [44–47]. Given the rapid expansion of research in this field and the urgent demand for practical, industrially relevant electrocatalysts, such a focused review is both timely and of considerable significance [48,49].

In this article, we provide a systematic and in-depth overview of recent advances in 2D Bi NSs for electrochemical CO_2 reduction. We first discuss the intrinsic challenges in controlled synthesis, followed by a comprehensive analysis of bottom-up, top-down, and vapor-phase strategies for preparing 2D Bi NSs. We then highlight state-of-the-art application strategies in CO_2RR, including defect and strain engineering, electronic modulation, interface design, hybrid architectures, and dynamic structural evolution. Special emphasis is placed on mechanistic insights gained from *in situ/operando* characterization and theoretical modeling, which bridge the gap between structural regulation and catalytic function. Finally, we summarize the current advances and provide perspectives on future research directions, including precise atomic-scale control, dynamic reconstruction, multi-scale architecture integration, product selectivity expansion, device-level design, and data-driven discovery. By consolidating the latest developments and offering forward-looking insights, this review aims to establish a roadmap for the rational design of 2D Bi NSs toward efficient, selective, and durable CO_2 electroreduction, thereby contributing to sustainable carbon utilization and energy transition.

2. Challenges in the controlled synthesis of 2D Bi NSs

The bottom-up controllable chemical synthesis of high-quality, monodisperse bismuth (Bi) nanocrystals, particularly two-dimensional (2D) nanostructures, remains highly challenging due to the intrinsic physicochemical properties of Bi and the limitations of conventional synthetic routes [50]. Compared with noble metals such as Au, Ag, Pt, and Pd, low-melting-point (LMP) main-group metals, including Bi, share several inherent features that hinder morphology control: (1) Low standard redox potential (difficult to reduce), (2) low melting point in both bulk and nanoscale phases (poor structural stability), and (3) low crystal symmetry (difficulty in forming well-defined nanocrystals). These attributes significantly alter their reduction, nucleation, crystallization, and growth mechanisms from those of noble metals, making it difficult to precisely control their composition, structure, and morphology *via* traditional bottom-up chemical methods [51].

(1) High chemical reactivity. The standard hydrogen electrode reduction potential of Bi^{3+}/Bi is only +0.20 V (or +0.32 V *vs.* SHE in aqueous solution [51–54]), much lower than that of Au^{3+}/Au (+1.52 V) or Ag^{+}/Ag (+0.80 V). This low potential renders Bi^{3+} reduction thermodynamically difficult and kinetically sluggish, often necessitating strong reducing agents (*e.g.*, $NaBH_4$, hydrazine hydrate) and/or high-temperature conditions to drive the process. However, such aggressive conditions severely limit the degree of control over precursor reduction, nucleation, and growth rates, ultimately resulting in broad size and shape distributions. (2) Low melting point. Bi has a bulk melting point of ~271 °C, with nanoscale Bi exhibiting even lower melting temperatures. Under typical high-temperature synthesis conditions for nanocrystals, the low thermal stability of Bi leads to uncontrollable growth and crystallization processes, further complicating morphology control. (3) Low crystal symmetry. Unlike *fcc*-structured Au, Ag, Pt, and Cu, or hcp-structured Ru, Bi crystallizes in a rhombohedral structure. This anisotropic crystal symmetry gives rise to unique growth pathways and facet development, which are less understood and far more difficult to manipulate using established metal nanocrystal growth strategies. (4) Unique surface adsorption behavior. Common surfactants (*e.g.*, CTAB, PVP) exhibit markedly different adsorption behavior on Bi surfaces compared to noble metals. Consequently, conventional "surface adsorption–induced" shape-control methods are less effective in the Bi system, leaving its nanocrystal morphology largely uncontrolled [51–54].

Conventional methods for Bi nanocrystal synthesis often involve strong reductants, elevated temperatures (>160 °C), and prolonged reaction times (hours to days) [51–54]. These harsh conditions frequently yield polydisperse products and hinder the preparation of monodisperse, high-quality, low-dimensional Bi nanocrystals with well-defined anisotropic morphologies. To address these issues, alternative approaches such as top-down exfoliation [55–58], physical vapor deposition or hot pressing [59–61], and electrochemical reduction of Bi-based compounds [62–70] have been explored. While these methods can bypass some of the challenges associated with direct chemical reduction, they still face limitations in achieving precise, simultaneous control over size, structure, and morphology at scale.

In summary, the synthesis of 2D Bi NSs remains constrained by the fundamental physicochemical characteristics of Bi and the inadequacies of current synthetic strategies. Overcoming these barriers requires the development of novel methodologies that integrate precise reaction control with a deep mechanistic understanding of Bi nucleation and growth.

3. Recent advances in the synthesis of 2D Bi NSs

In general, synthesis strategies for 2D Bi NSs can be categorized into two major classes: Bottom-up approaches, in which atomic or molecular precursors assemble into 2D structures (including chemical, electrochemical, and vapor-phase routes), and top-down approaches, where layered bulk Bi crystals are exfoliated into ultrathin sheets. Among bottom-up techniques, wet-chemical synthesis, reduction–melting–crystallization (RMC), and physical vapor deposition (PVD) represent typical solution- and vapor-based variants, respectively.

3.1. Bottom-up synthesis methods

Bottom-up synthesis relies on controlled chemical or physical processes to assemble atoms, ions, or molecules into ordered nanostructures. For 2D Bi NSs, these approaches offer fine tunability in thickness, crystallinity, and morphology, thereby tailoring the electronic structure and catalytic properties. Despite notable advances, each method still presents intrinsic advantages and challenges [71].

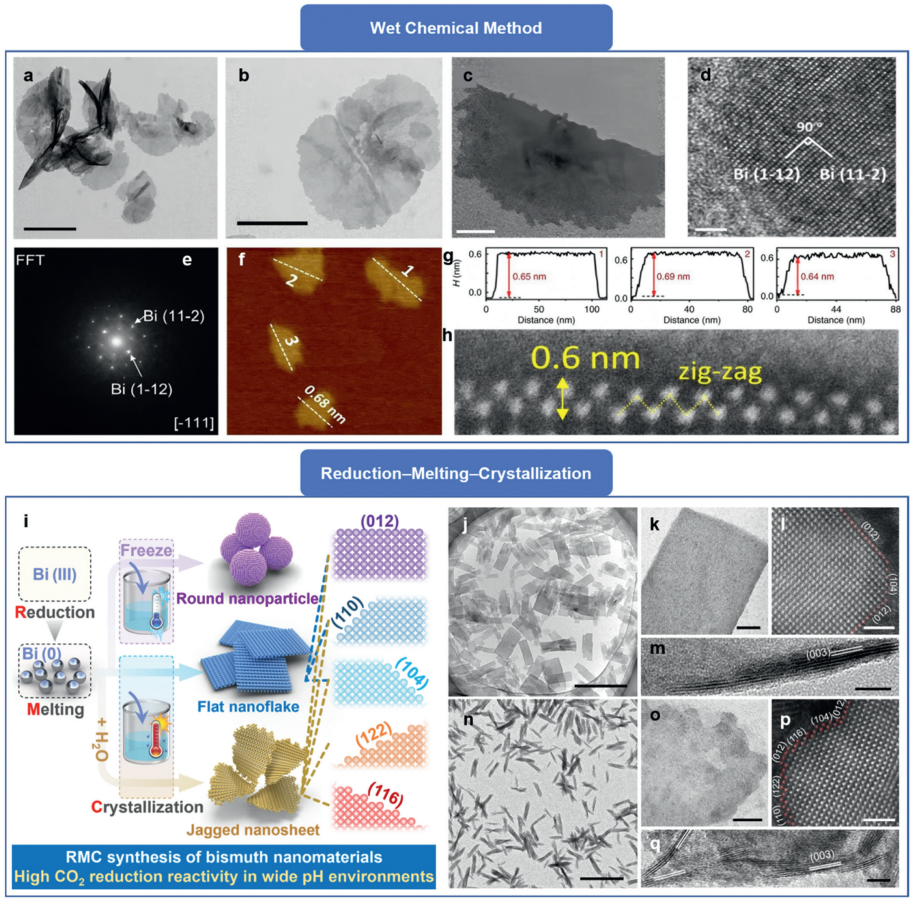


Fig. 1. Representative characterization of 2D Bi NSs synthesized *via* chemical reduction strategies. (a–c) Low- and high-magnification TEM images of ultrathin Bi NSs with wrinkled and flower-like morphologies. (d) HRTEM image revealing crystalline domains with a 90° lattice orientation relationship. (e) Corresponding FFT pattern indexed to Bi crystal planes. (f) AFM image of few-layer bismuthene nanosheets with uniform lateral size. (g) Thickness profiles along selected nanosheets (labeled 1–3), indicating a thickness of ~0.65–0.69 nm, consistent with single-atom-layer bismuthene. (h) HAADF-STEM image resolving the zig-zag atomic arrangement, directly demonstrating the atomic-scale thickness of the nanosheets. Reproduced with permission [72]. Copyright 2020, Springer Nature. (i) Schematic illustration of the reduction–melting–crystallization (RMC) pathway enabling morphology-controlled Bi nanostructures, including round nanoparticles, flat nanoflakes, and jagged nanosheets, with exposure of different crystallographic facets. (j–q) TEM and HRTEM images of the as-prepared Bi nanostructures, showing well-defined lattice fringes and facet orientation of Bi NSs with abundant high-index planes. Reproduced with permission [73]. Copyright 2023, Wiley-VCH.

3.1.1. Wet chemical method

The wet-chemical reduction method is one of the earliest strategies employed for fabricating ultrathin Bi NSs. Typically, $BiCl_3$ or other Bi salts serve as precursors, while strong reductants such as sodium borohydride ($NaBH_4$) are applied under controlled conditions. For instance, dropwise addition of $NaBH_4$ to $BiCl_3$ solution under argon atmosphere at ~120 °C produced freestanding nanosheets with tunable thickness down to the monolayer (~0.65 nm) [72].

This method is relatively simple, scalable, and yields nanosheets with high thermal stability and intact metallic Bi(0) character, as evidenced by TEM, AFM, and XPS analyses (Figs. 1a–h) [72]. The major drawback is poor morphological uniformity, stemming from the fast and uncontrolled reduction of Bi^{3+}, which induces aggregation and broad thickness distributions. Surfactant assistance is often insufficient due to the weak adsorption of common ligands on Bi surfaces [51–54]. Hence, further optimization in ligand chemistry and reductant choice is necessary for achieving monodisperse products.

3.1.2. Reduction–melting–crystallization (RMC, a liquid-phase variant of wet-chemical synthesis)

As a unique subset of wet-chemical synthesis, the Reduction–Melting–Crystallization (RMC) method exploits the intrinsically low melting point of bismuth to induce transient liquid-phase intermediates and controlled recrystallization, thereby offering morphology-tunable nanosheet formation. In this process, bismuth acetate is reduced in ethylene glycol at 470 K, leading to transient liquefied Bi droplets owing to its low melting point. Rapid cooling in ethanol favors spherical nanoparticle formation, whereas slower crystallization yields flat nanoflakes (*f*-BiNFs). Introduction of trace water further induces structural perturbations, giving rise to jagged nanosheets (*j*-BiNSs) rich in surface defects (Figs. 1i–q) [73].

The RMC method enables precise morphology modulation, surfactant-free surfaces, and versatile nanosheet architectures. TEM, XRD, and Raman indicate ultrathin structures of 1.9–2.8 nm with metallic Bi(0) phase [73]. The method demands strict control over reaction temperature, cooling rate, and inert atmosphere. Moreover, scalability remains a challenge, limiting its industrial applicability. Nevertheless, the concept of exploiting Bi's low melting point to guide morphology evolution provides valuable mechanistic insights for future synthesis [74].

3.1.3. Electrochemical reduction of bismuth compounds

Electrochemical reduction of layered bismuth precursors, such as BiOX (X = Cl, Br, I), $Bi_2O_2CO_3$, or Bi-based MOFs, has recently emerged as an effective strategy to obtain two-dimensional metallic Bi NSs while preserving the structural characteristics of the original compounds [75]. For example, Zhu and Xu developed an electrochemical conversion route from Bi-based layered MOFs

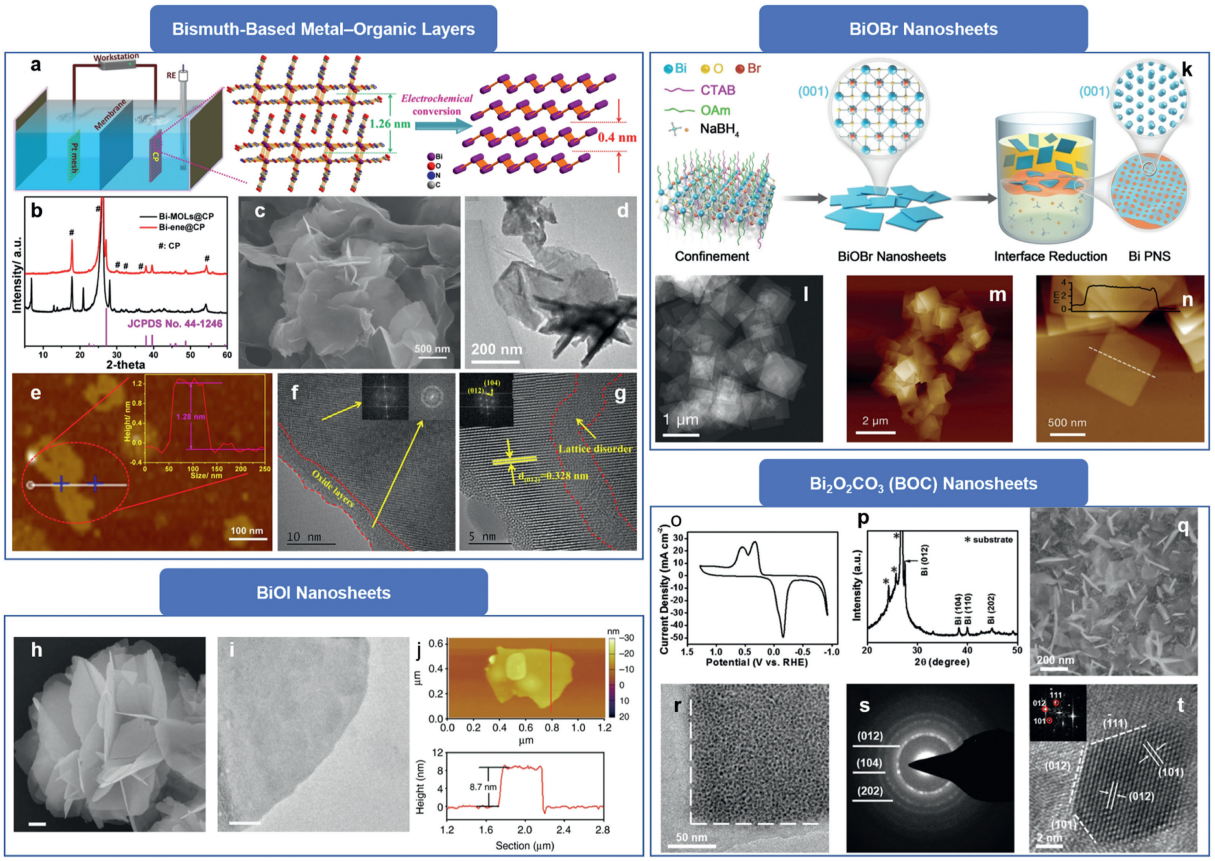


Fig. 2. Electrochemical reduction–derived synthesis and structural characterizations of Bi-based nanosheets. (a) Schematic illustration of the electrochemical conversion of Bi metal–organic layers (Bi-MOLs) into ultrathin Bi NSs (Bi-ene), highlighting the layer-to-layer transformation pathway. (b) PXRD patterns showing the crystalline evolution from Bi-MOLs to Bi-ene. (c, d) SEM and TEM images showing the sheet-like morphology of Bi-ene. (e) AFM image with corresponding thickness profile (~1.26 nm), verifying the ultrathin structure. (f, g) HRTEM images with selected area electron diffraction (SAED), indicating the presence of lattice disorder and exposed high-index facets. Reproduced with permission [69]. Copyright 2020, Wiley-VCH. (h–j) Structural characterization of BiOI-derived nanosheets, including SEM, TEM, and AFM analyses, revealing ultrathin morphology with thickness of ~8.7 nm. Reproduced with permission [67]. Copyright 2018, Springer Nature. (k) Schematic illustration of the chemical interface confinement reduction of BiOBr nanosheets into porous Bi NSs (Bi PNS). (l–n) HAADF-STEM and AFM images of Bi PNS, together with height profile, demonstrating controlled nanosheet thickness and porous architecture. Reproduced with permission [70]. Copyright 2021, Wiley-VCH. (o–p) XRD patterns and SEM images of $Bi_2O_2CO_3$ (BOC) precursors. (q–r) TEM images and SAED patterns, together with (s–t) AFM images and thickness profiles, validating the structural reconstruction from BOC precursors into Bi NSs under electrochemical reduction. Reproduced with permission [66]. Copyright 2018, Wiley-VCH.

to bismuthene with a thickness of 1.28–1.45 nm. The resulting nanosheets exposed abundant low-coordinated sites and demonstrated near-unity Faradaic efficiency for formate production over a wide potential window, while maintaining excellent operational stability (Figs. 2a–g) [69]. Similarly, Yafei Li and Yanguang Li achieved the topotactic transformation of BiOI templates into ultrathin Bi NSs under cathodic polarization, with theoretical calculations suggesting that the exposed Bi(001) planes preferentially stabilized the *OCHO intermediate and thus promoted selective formate formation (Figs. 2h–j) [67]. In another representative work, a scalable chemical interface confinement reduction strategy was reported for the topotactic transformation of BiOBr nanosheets into porous Bi(001) nanosheets, which delivered a Faradaic efficiency of 95.2 % and a formate partial current density of 72 mA/cm^2, with density functional theory (DFT) analysis revealing that the exposed (001) facets and small-angle grain boundaries substantially lowered the free energy barrier for *OCHO formation (Figs. 2k–n) [70]. Likewise, Lu and Li reported the *in situ* reduction of ultrathin $Bi_2O_2CO_3$ nanosheets into mesoporous Bi, which exhibited enlarged surface area and outstanding catalytic activity for CO_2RR (Figs. 2o–t) [66].

Compared with conventional chemical reduction, this electrochemical approach offers the advantage of structural fidelity, as the two-dimensional framework of the precursors is largely retained during the transformation. Moreover, the process is inherently compatible with *operando* spectroscopic techniques (*e.g.*, ATR-IR, Raman), which allows mechanistic insights into structural evolution and intermediate stabilization. The direct integration with electrochemical CO_2 reduction systems further underscores its practical relevance. Nevertheless, challenges remain. Structural reconstruction during the reduction process may induce partial collapse of the layered framework, leading to morphological heterogeneity, while precise control of nanosheet thickness and uniformity over large electrode areas is still difficult to achieve. These limitations highlight the need for more refined electrochemical design strategies, such as electrolyte engineering or potential-programming, to fully exploit the potential of this method [76].

3.1.4. Physical vapor deposition and termal techniques

In addition to chemical and exfoliation strategies, physical vapor deposition (PVD) and thermal-based methods provide an alternative route for synthesizing ultrathin Bi NSs and bismuthene films. Owing to the intrinsically low melting point of Bi (271.5 °C in bulk, even lower at the nanoscale) [51], physical and thermal techniques are capable of producing highly crystalline, few-layer structures under relatively mild conditions compared to conventional high-temperature crystal growth [77].

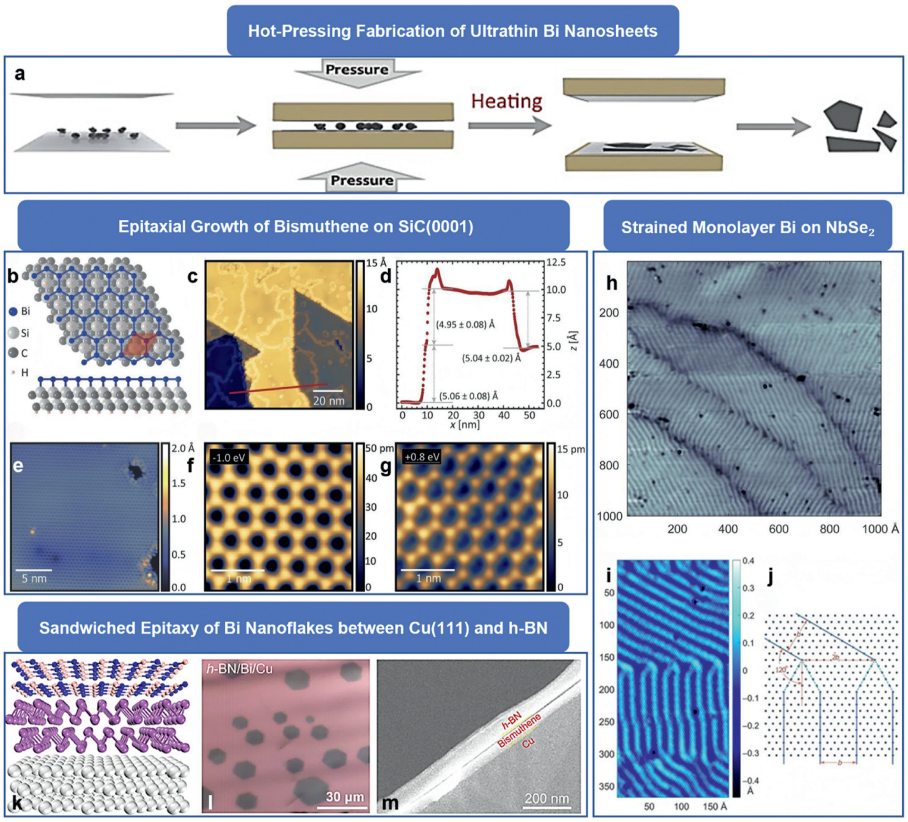


Fig. 3. Physical vapor deposition and thermal-assisted routes for fabricating 2D Bi NSs. (a) Schematic illustration of the hot-pressing fabrication of ultrathin Bi NSs using pristine Bi nanoparticles under simultaneous heating and pressure, enabling controlled melting–recrystallization into atomically thin sheets. Reproduced with permission [59]. Copyright 2017, Wiley-VCH. (b–g) Epitaxial growth of bismuthene on SiC(0001). Reproduced with permission [60]. Copyright 2017, AAAS. (b) Structural model of bismuthene with a $(\sqrt{3}\times\sqrt{3})$R30° commensurate registry on the SiC(0001) substrate. (c) STM topographic image showing continuous bismuthene domains (~25 nm) fully covering the substrate. (d) Step-height profile taken along the red line in (c), consistent with the SiC terrace steps. (e) Atomically resolved STM image revealing a honeycomb Bi lattice. (f, g) High-resolution STM images under occupied (−1.0 eV) and empty (+0.8 eV) states, respectively, revealing the buckled honeycomb configuration of bismuthene. Strained monolayer Bi on $NbSe_2$: (h) Large-scale STM image showing periodic ripple morphology with a modulation period of ~5 lattice constants. (i) Atomically resolved topography (180 Å × 360 Å) highlighting triangular Bi lattice, ripple-induced strain, and Y-type domain junctions. (j) Schematic illustration of the geometric constraints leading to Y-junction formation.Reproduced with permission [61]. Copyright 2018, AAAS. Sandwiched epitaxial growth of Bi nanoflakes between Cu(111) and h-BN: (k) Schematic diagram of the h-BN–encapsulated epitaxial growth process, where the h-BN overlayer prevents oxidation and enables layer-by-layer Bi growth on Cu foil. (l) Optical and SEM images showing uniform Bi nanoflakes confined between h-BN and Cu substrate. (m) Cross-sectional SEM image of the h-BN/Bi/Cu sandwich structure, demonstrating ultrathin Bi layer formation. Reproduced with permission [78]. Copyright 2023, American Chemical Society.

One representative thermal approach was reported by Wu and co-workers, who developed a hot-pressing strategy to fabricate freestanding ultrathin Bi NSs with a thickness of ≈2 nm and lateral dimensions of several micrometers [59]. In this process, Bi nanoparticles were mechanically compressed onto polished Si substrates, enabling ordered crystallization into high-quality nanosheets. This cost-effective method demonstrated great promise for large-scale fabrication, while simultaneously ensuring high crystallinity and mechanical integrity.

Beyond mechanical pressing, vapor deposition and epitaxial growth strategies have also been developed to achieve atomic-level control in bismuthene synthesis. Unlike freestanding nanosheets obtained by hot-pressing (Fig. 3a) [59], vapor deposition enables the direct fabrication of monolayer Bi on crystalline substrates under low-pressure conditions. In 2017, Schäfer and co-workers epitaxially grew monolayer bismuthene on SiC substrates using a physical evaporation–deposition method, as validated by scanning tunneling microscopy (STM) and step-height analysis (Figs. 3b–g) [60]. Shortly thereafter, Kapitulnik and colleagues employed a Knudsen cell to deposit Bi atomic layers on $NbSe_2$ substrates (Figs. 3h–j) [61]. Their study revealed that the initial Bi growth was epitaxially aligned with the lattice constant of the top-layer Se atoms of $NbSe_2$, forming a rippled 2D Bi lattice with a periodicity of approximately five unit cells. Although these methods enabled precise growth of monolayer bismuthene, the resulting nanosheets remained substrate-supported at the macroscopic scale, which restricted their practical application due to substrate dependence.

More recently, a “sandwiched epitaxy” strategy was reported, in which Bi was confined between a Cu(111) foil substrate and an h-BN protective overlayer (Figs. 3k–m) [78]. The h-BN layer not only stabilized the otherwise metastable bismuthene by suppressing structural reconstruction, but also compensated for charge transfer to the Cu substrate. As a result, the bismuthene nanoflakes demonstrated remarkable thermal stability up to 500 °C in air, attributed to the passivation effect of the h-BN capping layer. Importantly, these nanoflakes exhibited an ultrahigh faradaic efficiency (≈96.3 %) for formate production in CO_2RR, one of the highest values reported for Bi-based electrocatalysts. This strategy not only enables controllable synthesis of high-quality 2D bismuthene but also provides a generalizable route for stabilizing other 2D materials with intrinsically high surface energies.

Compared with chemical reduction or exfoliation, physical vapor deposition and thermal strategies offer distinct advantages. They enable the synthesis of large-area, high-crystallinity nanosheets with atomically smooth surfaces, which are highly desirable for fundamental studies and device integration. Moreover, these approaches are well-suited for *in situ* monitoring and structural characterization, since they avoid complications introduced

by surfactants or residual ligands. However, these methods also face significant challenges. Substrate dependency limits their scalability and versatility, as most epitaxial growth requires lattice-matched templates. In addition, while high crystallinity is beneficial for electronic applications, catalytic systems often demand defect-rich structures with abundant low-coordination sites, which are difficult to achieve through purely thermal growth.

In summary, physical vapor deposition and thermal techniques represent powerful tools for the controllable synthesis of 2D Bi NSs, particularly for producing structurally coherent and high-quality bismuthene. Nevertheless, bridging the gap between substrate-supported epitaxial growth and freestanding, defect-engineered nanosheets remains a critical challenge that must be addressed before these approaches can be broadly applied in large-scale electrocatalytic systems.

3.2. Top-down exfoliation approaches

Unlike bottom-up chemical methods that rely on precursor reduction or crystallization, top-down strategies exploit the intrinsic layered structure of bulk bismuth crystals to obtain ultrathin nanosheets through mechanical or chemical exfoliation. This approach is conceptually analogous to the production of graphene from graphite, and it benefits from the weak van der Waals interactions between Bi atomic layers that facilitate cleavage into two-dimensional structures [79].

One of the earliest demonstrations was reported by Jin and co-workers, who successfully synthesized ultrathin Bi NSs with a thickness of 1.2–1.5 nm *via* liquid-phase exfoliation of bulk Bi in NaOH–isopropanol solution (Figs. 4a–g) [56]. The as-prepared nanosheets displayed high electrical conductivity and a large electrochemically active surface area, resulting in excellent CO_2 adsorption and rapid electron transport. DFT calculations further revealed that the abundant edge sites on these exfoliated nanosheets play a decisive role in stabilizing the key *OCOH intermediate, thereby accounting for the high formate selectivity observed in CO_2RR.

Building upon this work, Yin and co-workers developed a solvothermal–liquid-phase exfoliation strategy, which allowed precise control over nanosheet thickness and porosity through tuning of ligands, reducing agents, and reaction rates (Figs. 4h–m) [58]. The resulting ultrathin porous Bi NSs (≈1.5 nm thick) possessed numerous low-coordinated edge sites, significantly enhancing their intrinsic catalytic activity compared to Bi nanoparticles dominated by basal planes. These studies collectively highlight the structural advantages of exfoliation-derived Bi NSs, including ultrathin morphology, high surface-to-volume ratio, and abundant catalytically active edges.

From a mechanistic perspective, the principal advantage of exfoliation lies in its ability to generate atomically thin nanosheets without altering the crystallographic integrity of Bi. Furthermore, because it does not involve harsh reductants or extreme reaction conditions, the method produces relatively clean surfaces, minimizing interference from surfactant residues. However, several limitations hinder its broader application. First, the lateral dimensions and thickness distribution of exfoliated Bi NSs often suffer from poor uniformity, particularly at larger scales, which complicates reproducibility and device integration. Second, the yield of monolayer or few-layer nanosheets remains relatively low, and the process can be inefficient for mass production. Finally, the mechanical instability of ultrathin Bi layers under ambient conditions raises concerns about long-term structural preservation, especially in catalytic environments [80].

Overall, top-down exfoliation provides an accessible pathway to ultrathin Bi NSs with well-preserved crystal structures and abundant edge sites, making it a valuable complement to bottom-up chemical synthesis. Nevertheless, further refinement in exfoliation

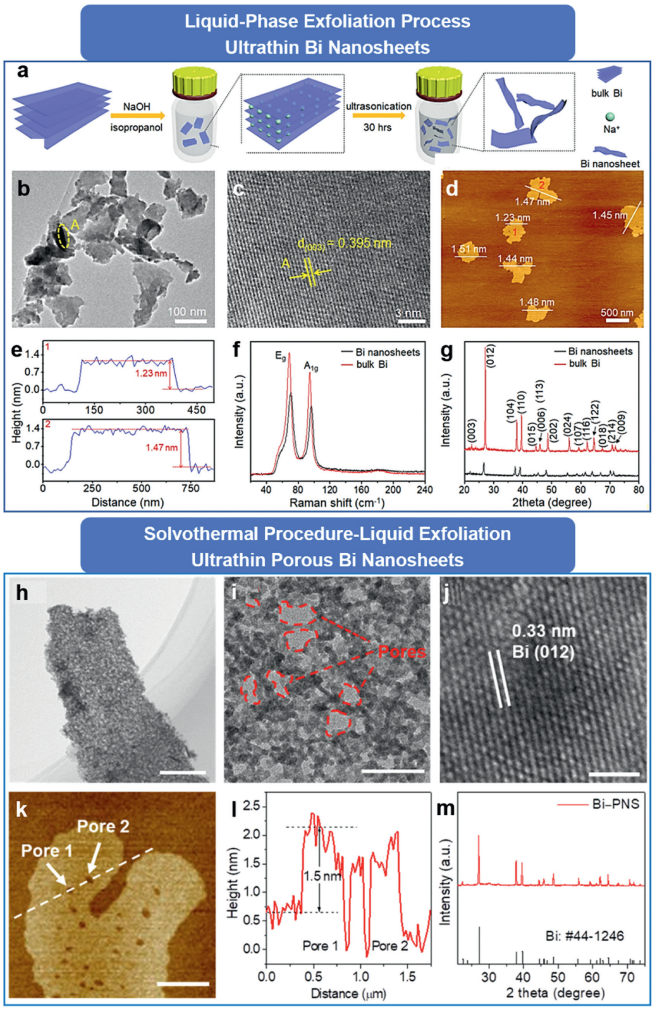


Fig. 4. Top-down exfoliation strategies for preparing ultrathin Bi NSs and their structural characterizations. (a) Schematic illustration of the scalable liquid-phase exfoliation process to obtain ultrathin Bi NSs. (b, c) TEM and HRTEM images of the exfoliated products reveal few-layer Bi with well-resolved lattice fringes. (d, e) AFM image and corresponding height profiles further verify the ultrathin thickness distribution. (f, g) Raman spectra and XRD patterns of exfoliated nanosheets compared with bulk Bi, demonstrating structural integrity and layer reduction. Reproduced with permission [56]. Copyright 2018, Elsevier. Morphological and structural features of porous Bi NSs (Bi-PNS) obtained by exfoliation: (h, i) TEM and magnified TEM images reveal the porous sheet-like morphology. (j) HRTEM image showing crystalline lattice fringes. (k, l) AFM image and the corresponding height profile demonstrate the nanosheet thickness at the few-nanometer scale. (m) XRD patterns indicate the phase composition of exfoliated Bi-PNS. Reproduced with permission [58]. Copyright 2022, American Chemical Society.

chemistry and post-processing strategies is needed to improve size control, scalability, and structural stability, thereby unlocking its full potential for electrocatalytic applications.

3.3. Summary and perspectives on synthesis approaches

Over the past decade, significant progress has been achieved in the synthesis of two-dimensional bismuth (Bi) nanosheets through a variety of strategies, including bottom-up chemical routes, top-down exfoliation techniques, and physical vapor deposition (PVD) or thermal-based methods (Table 1). Each approach offers unique advantages while simultaneously facing intrinsic limitations, which collectively highlight the complexity of achieving precise control over Bi nanostructures [81].

Bottom-up chemical methods, encompassing wet chemical reduction, reduction–melting–crystallization (RMC), and electro-

Table 1
Comparative summary of synthesis strategies for 2D Bi nanosheets.

Synthesis method	Representative strategy	Key advantages	Main limitations
Wet-chemical reduction	Direct reduction of Bi^{3+} salts (*e.g.*, $BiCl_3 \rightarrow Bi^0$) using $NaBH_4$ or hydrazine	Simple, scalable; surfactant-assisted morphology control; freestanding Bi NSs	Poor uniformity due to rapid reduction kinetics; aggregation; broad thickness distribution
Reduction–melting–crystallization (RMC)	Controlled reduction near Bi melting point to induce transient liquid-phase intermediates	Tunable morphology (nanoflakes, jagged NSs); surfactant-free surfaces; mechanistic insight into Bi melting behavior	Requires precise control of temperature/cooling; limited scalability
Electrochemical reduction of Bi compounds	Topotactic transformation of BiOX, $Bi_2O_2CO_3$, or Bi-MOFs under cathodic bias	Structural fidelity; *operando* compatibility; direct integration with CO_2RR	Morphological heterogeneity; partial collapse of frameworks; difficult large-area uniformity
Physical vapor deposition/thermal routes	Hot pressing, epitaxial growth (SiC, $NbSe_2$), or h-BN encapsulation	High crystallinity; atomic-level precision; surfactant-free; ideal for mechanistic studies	Substrate dependency; limited defect density; not freestanding
Top-down exfoliation	Mechanical or liquid-phase cleavage of bulk Bi crystals	Clean surfaces; abundant edge sites; defect-rich active structures	Low yield; poor size/thickness uniformity; limited long-term stability

chemical transformation of Bi-based precursors, have demonstrated remarkable versatility in tuning the morphology, porosity, and surface chemistry of Bi NSs. These methods are particularly attractive for their potential scalability and direct integration with electrocatalytic CO_2 reduction systems. Nevertheless, the inherently low redox potential of Bi^{3+}/Bi necessitates the use of strong reductants or high-temperature conditions, often resulting in broad size distributions and structural heterogeneity. Moreover, achieving precise control over nanosheet thickness at the atomic level remains challenging, which limits their reproducibility in catalytic studies.

In contrast, top-down exfoliation approaches exploit the layered crystal structure of bulk Bi to directly obtain ultrathin nanosheets. This class of methods benefits from simplicity, minimal use of harsh chemicals, and the generation of defect-rich edges that are advantageous for catalysis. However, exfoliation often suffers from low yield, poor control over lateral dimensions and thickness distribution, and difficulty in scaling up for practical applications. While solvothermal–liquid phase exfoliation has improved nanosheet quality and porosity, it remains insufficient to fully meet the demands of large-area and uniform Bi nanosheet fabrication [82].

PVD and thermal techniques, including hot-pressing, epitaxial deposition, and sandwiched epitaxy, have enabled the preparation of ultrathin Bi NSs and bismuthene with atomic-level precision and high crystallinity [83]. These methods are particularly valuable for fundamental studies, as they allow the synthesis of monolayer structures on well-defined substrates and facilitate *operando* structural characterization. Furthermore, recent sandwiched epitaxy strategies have achieved outstanding thermal stability and record-high faradaic efficiency in CO_2RR, underscoring the potential of substrate-engineered growth. However, these approaches are heavily substrate-dependent, and the resulting nanosheets are often not freestanding, which limits their scalability and applicability in practical catalytic devices. In addition, defect engineering, critical for optimizing electrocatalytic performance, is more difficult to realize within purely epitaxial growth frameworks [84].

Taken together, these synthesis approaches highlight a fundamental trade-off between structural precision, scalability, and catalytic relevance. Chemical reduction and exfoliation excel in generating defect-rich, catalytically active structures but struggle with uniformity and large-scale reproducibility [85]. By contrast, PVD and epitaxial methods deliver atomic-level control and high crystallinity but remain constrained by substrate dependency and limited applicability in electrocatalysis. Addressing these challenges will require the development of hybrid strategies that integrate the advantages of different synthesis paradigms—for example, combining scalable bottom-up synthesis with post-synthetic exfoliation or defect engineering, or leveraging epitaxial templates to seed freestanding nanosheet growth [86].

Most importantly, the choice of synthesis method directly dictates the structural characteristics of Bi NSs, including thickness, defect density, crystallinity, and surface termination, which in turn govern their catalytic activity, selectivity, and stability in CO_2RR [87]. Therefore, establishing a clear synthesis–structure–performance relationship is essential for advancing Bi-based electrocatalysts. This critical understanding provides the conceptual bridge to the following section, where we focus on application strategies and design principles for Bi NSs in CO_2 electroreduction [88].

4. Application strategies of 2D Bi NSs in electrochemical CO_2 reduction

To provide a comprehensive framework for understanding how structural and electronic regulations improve the catalytic behavior of two-dimensional Bi NSs, Fig. 5 summarizes the key design strategies that have been developed for optimizing their performance in electrochemical CO_2 reduction. Each strategy targets specific limitations of pristine Bi NSs, such as limited active-site density, sluggish electron transfer, and structural instability, and offers a distinct route to enhance activity, selectivity, and durability.

First, defect engineering and strain modulation create undercoordinated and lattice-distorted Bi sites that strengthen CO_2 adsorption and facilitate the formation of OCHO intermediates, thereby accelerating the rate-determining step. Second, heteroatom doping and interface engineering adjust the local electronic structure and promote charge redistribution across Bi–O or Bi–M boundaries, stabilizing key intermediates while suppressing competing hydrogen evolution. Third, integration with conductive supports or heterostructures improves charge and mass transport, providing efficient electron pathways and mechanical robustness under high current densities. Fourth, *in situ* reconstruction activates metastable or amorphous Bi phases that expose fresh low-coordinated Bi sites during operation, often leading to enhanced long-term stability. Finally, microenvironment and reaction-condition engineering—including electrolyte composition, local pH, and ion effects, further tunes the adsorption–desorption equilibria and facilitates the continuous conversion of CO_2 to formate.

Together, these seven regulatory strategies form a unified design paradigm for 2D Bi NSs, linking atomic-level structure modulation with macroscopic catalytic behavior. This integrative perspective provides a conceptual bridge from synthesis fundamentals

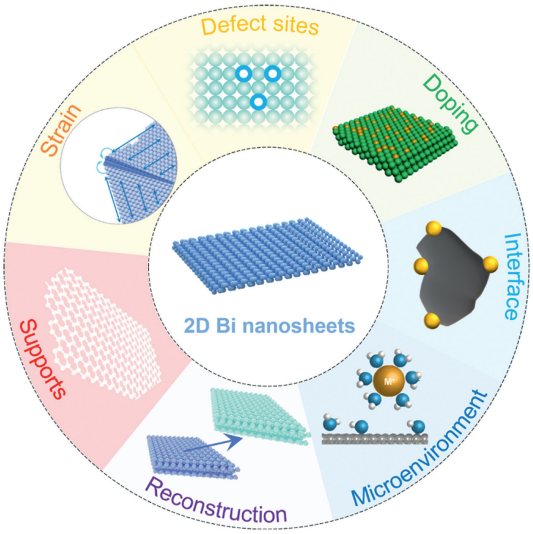


Fig. 5. Schematic illustration of the application strategies of two-dimensional (2D) Bi NSs in electrochemical CO_2 reduction. Seven representative approaches have been developed to optimize catalytic activity, selectivity, and durability: (1) Introduction of defect sites to create coordinatively unsaturated active centers; (2) Strain engineering to modulate the electronic structure and lower energy barriers; (3) Doping strategies for electronic modulation and stabilization of intermediates; (4) Interface engineering to construct hybrid Bi/Bi–O architectures with synergistic effects; (5) Integration with conductive supports to enhance charge transport and mass transfer; (6) *In situ* reconstruction and dynamic evolution to expose highly active phases; (7) Tailoring of the microenvironment (*e.g.*, electrolyte composition, ion effects, and local pH) to promote CO_2 adsorption and conversion. Collectively, these strategies highlight the versatility of 2D Bi NSs as a platform for designing next-generation electrocatalysts toward efficient and sustainable CO_2-to-formate conversion.

(Section 3) to the detailed application discussions in the following subsections (Sections 4.1–4.8). Overall, the schematic in Fig. 5 provides a unified perspective on how different structural and electronic tuning routes govern the catalytic behavior of 2D Bi NSs. The following subsections (Sections 4.1–4.8) will discuss each strategy in detail with representative examples.

4.1. Creation of under-coordinated sites

The formation of under-coordinated Bi sites, including edge atoms, vacancies, and dislocations, has emerged as one of the most effective strategies to enhance the intrinsic activity of two-dimensional Bi NSs for CO_2 reduction. Owing to their low coordination number, these sites exhibit modified local electronic structures that stabilize the key *OCHO intermediate, suppress competitive hydrogen evolution, and thereby boost the selectivity toward formate. Both theoretical calculations and spectroscopic studies consistently point to the strong correlation between the density of unsaturated sites and CO_2RR performance [89].

For instance, defect-rich Bi NSs with lattice dislocations supported on copper foam were fabricated *via* a combined etching–oxidation–reduction route, and the catalytic efficiency was further amplified by introducing nanobubble technology (Fig. 6a) [90]. This integrated system achieved a high formate Faradaic efficiency of 95.4 % at −1.08 V *vs.* RHE, with an impressive energy efficiency of ~60 %, while nanobubble-assisted mass transport accelerated CO_2 conversion nearly fivefold. Similarly, atomic vacancies introduced into Bi NSs derived from electrochemically reduced $Bi_2O_2CO_3$ facilitated an electron-rich surface, shifting the Bi p-band states toward the Fermi level (Fig. 6b) [55]. This modification significantly lowered the activation barrier for CO_2 activation and stabilized OCHO* intermediates through enhanced p–O orbital hybridization, yielding a Faradaic efficiency of 90 % at only 420 mV overpotential with remarkable 100 h durability.

Edge site engineering further highlighted the critical role of unsaturated coordination. Ligand-assisted stabilization of under-coordinated Bi sites has been demonstrated using *in situ* reduction of Bi-based MOFs (Fig. 6c) [91]. The resulting ligand-stabilized nanosheets exhibited nearly quantitative formate selectivity (98 %) at −0.80 V *vs.* RHE with excellent stability over 40 h, highlighting the synergistic effect of ligand anchoring in preventing site collapse. By controlling topotactic transformation pathways, Bi NSs enriched with edges and defects achieved record-breaking industrially relevant current densities, reaching ~870 mA/cm^2 in flow-cell devices while maintaining >90 % formate selectivity (Fig. 6d) [92]. In addition, *in-situ* FTIR analyses [92] captured the accumulation of *OCHO species, which—together with DFT calculations—suggest that OCHO formation on edge defects is energetically favored over terrace atoms. Beyond defect introduction, molten-salt-assisted synthesis has been employed to produce high-yield Bi NSs with inherently exposed edge sites (Fig. 6e) [93]. These catalysts delivered outstanding long-term stability, continuously operating for one month in a flow cell, with a remarkable formate yield rate of 787.5 mmol cm^{-2} h^{-1}.

Taken together, these studies illustrate that unsaturated coordination environments, whether generated by dislocations, atomic vacancies, edges, or ligand stabilization—consistently serve as dominant active sites for CO_2-to-formate conversion [94]. Despite these advances, challenges remain in quantitatively correlating the density and type of under-coordinated sites with catalytic activity, and in developing scalable synthesis approaches that allow fine-tuned control over these features without compromising stability. Future work should focus on *operando* spectroscopic investigations and predictive modeling to establish clear structure–activity relationships, which will guide rational design of defect-engineered Bi NSs with industrially viable CO_2RR performance.

4.2. Lattice distortion and strain engineering

Lattice strain represents a powerful structural lever to regulate the local coordination environment and electronic properties of Bi NSs, thereby tailoring their activity for CO_2 electroreduction. Unlike noble metals with rigid lattice frameworks, the relatively low symmetry and weak metallic bonding of Bi make its crystal lattice highly adaptable to distortions induced by synthetic conditions, defect generation, or support interactions. These distortions modulate orbital overlap and band structures, altering the adsorption free energies of key intermediates ($*CO_2^-$, *OCHO) and consequently the selectivity and kinetics of CO_2RR toward formate.

Tensile strain has proven highly effective in activating inert Bi sites and modulating the OCHO intermediate stabilization pathway (Fig. 7a) [95,96]. Through a rapid thermal shock process of a Bi-based MOF, small Bi clusters were generated, inducing vacancies that imposed tensile strain across adjacent non-defective Bi regions. This extended strain field lowered the reaction barrier for OCHO formation, resulting in remarkable CO_2RR performance: A formate FE of 96 % at 400 mA/cm^2 in acidic electrolyte, and nearly 1 A/cm^2 partial current density with high single-pass carbon efficiency (62 %). Furthermore, integration into a Zn–CO_2 battery achieved a peak power density of 21.4 mW/cm^2 and excellent durability, underscoring the practical potential of tensile-strain-engineered Bi NSs.

In contrast, compressive strain can also play a decisive role in optimizing CO_2 adsorption and intrinsic catalytic activity (Fig. 7b) [97,98]. Low-crystallinity $Bi_2O_2CO_3$ precursors underwent rapid electrochemical reduction, yielding lattice-distorted Bi NSs (Bi NS-L) with significant compressive strain, whereas highly crystalline precursors produced more ordered Bi NS-H structures. The com-

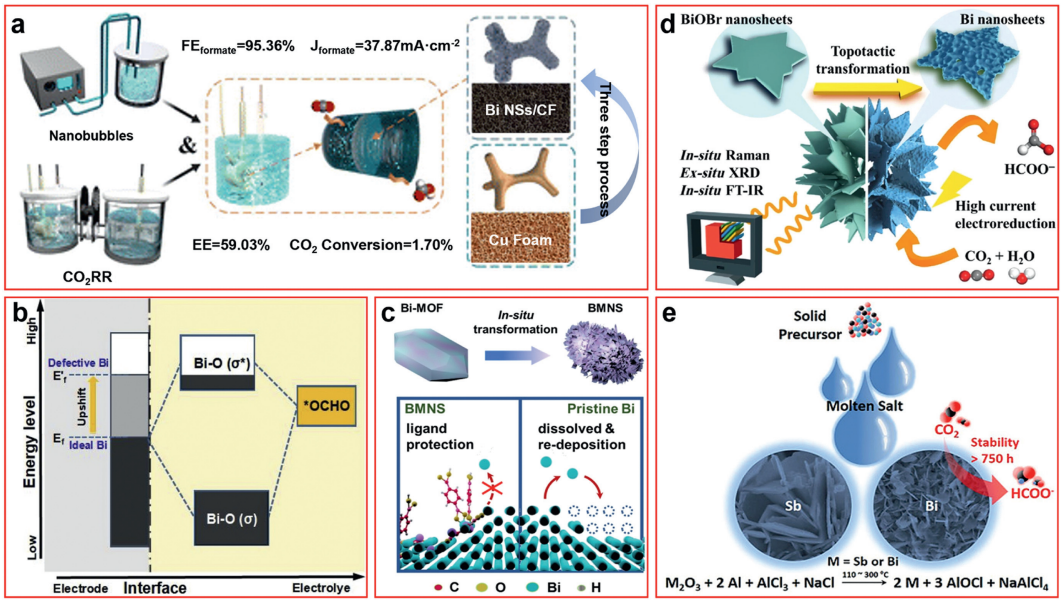


Fig. 6. Engineering of under-coordinated active sites in 2D Bi NSs for CO_2 electroreduction. (a) Bi NSs with abundant lattice dislocations constructed on copper foam *via* chemical etching–oxidation–reduction, achieving high $FE_{formate}$ (95.4 %) and improved CO_2 conversion efficiency, with nanobubble technology further accelerating mass transport and intermediate stabilization. Reproduced with permission [90]. Copyright 2024, Royal Society of Chemistry. (b) Electrochemically reduced $Bi_2O_2CO_3$ nanosheets with dominant (001) facets and Bi atom vacancies, where vacancy-induced electronic redistribution lowers the activation barrier for $^*CO_2^-$ and stabilizes *OCHO intermediate. Reproduced with permissions [55]. Copyright 2020, Elsevier. (c) Ligand-stabilized Bi NSs derived from *in situ* reduction of Bi-MOFs, where residual organic ligands effectively stabilize under-coordinated Bi sites, affording a high Faradaic efficiency of 98 % and enhanced durability. Reproduced with permission [91]. Copyright 2021, Elsevier. (d) Defect-rich Bi NSs obtained by topotactic transformation, where preferential exposure of edge sites enables ultra-high current density (~870 mA/cm^2) and high selectivity (>90 % FE) through facilitated *OCHO stabilization. Reproduced with permission [92]. Copyright 2023, Springer Nature. (e) Molten-salt-assisted aluminothermic reduction strategy for preparing Bi NSs with abundant edge sites, exhibiting superior long-term CO_2-to-formate conversion at industrially relevant current densities. Reproduced with permission [93]. Copyright 2020, Wiley-VCH.

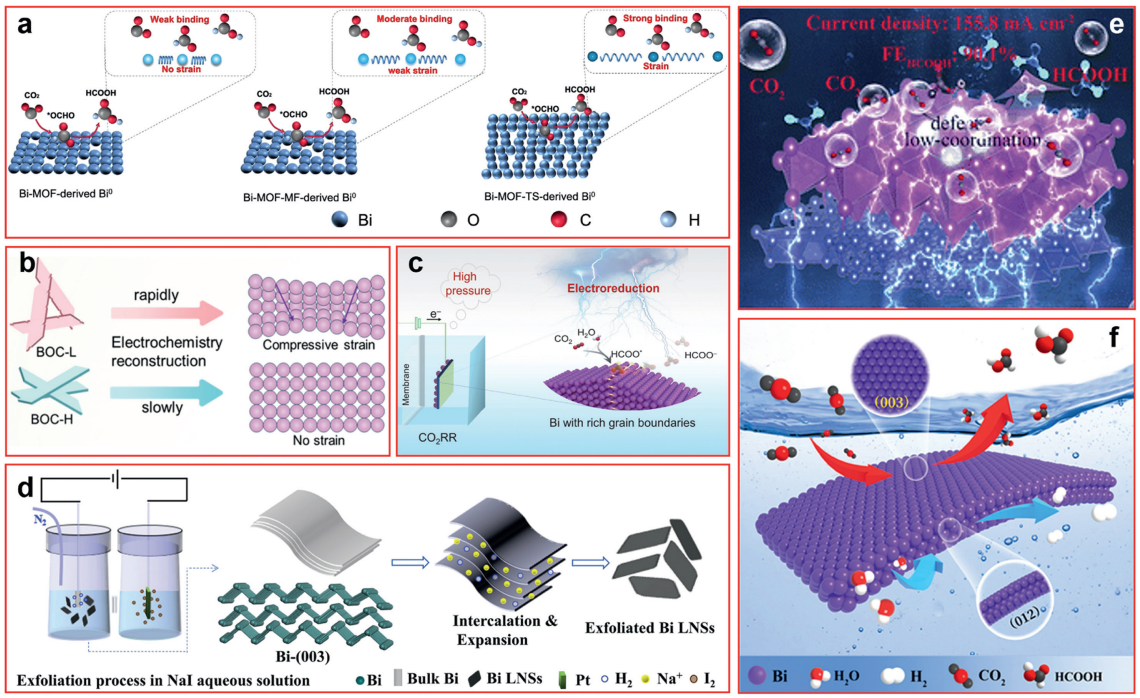


Fig. 7. Lattice distortion and strain engineering strategies in 2D Bi NSs for enhanced CO_2 electroreduction. (a) Post-reconstructed Bi^0 nanosheets with tunable strain states, where compressive strain optimizes the binding strength of OCHO intermediates, thereby promoting CO_2-to-formate conversion. Reproduced with permission [96]. Copyright 2025, Springer Nature. (b) Low-crystallinity $Bi_2O_2CO_3$-derived Bi NSs exhibiting compressive lattice distortion (Bi NS-L) outperform high-crystallinity Bi NS-H due to enhanced CO_2 adsorption and intrinsic activity, achieving >94 % $FE_{formate}$ at −1.08 V. Reproduced with permission [97]. Copyright 2025, American Chemical Society. (c) $BiPO_4$-derived nanosheets formed under high CO_2 pressure (3.0 MPa) with abundant grain boundaries, which induce charge redistribution, facilitate CO_2 activation, and stabilize HCOO intermediates for selective formate production (FE ≈ 90 %, $j_{formate}$ = 534 mA/cm^2). Reproduced with permission [99]. Copyright 2022, Elsevier. (d) Electrochemically exfoliated Bi lattice-distorted nanosheets (LNSs), where defect-rich atomic configurations provide high surface strain and increase active site density. Reproduced with permission [100]. Copyright 2021, Wiley-VCH. (e) 3D Bi NSs@Cu nanowire core–shell architectures exposing defect-rich Bi(110) facets, where atomic defects and lattice distortion synergistically enhance CO_2 adsorption and hydrogenation, enabling 155.8 mA/cm^2 current density with 90 % $FE_{formate}$. Reproduced with permission [101]. Copyright 2023, Royal Society of Chemistry. (f) Orientation-dependent Bi NSs obtained from topotactic reduction, revealing that basal-plane-oriented Bi NSs outperform edge-oriented ones by suppressing competing HER and lowering free-energy barriers for CO_2RR on strained basal planes. Reproduced with permission [102]. Copyright 2021, Elsevier.

pressive distortion facilitated CO_2 activation and enhanced OCHO stabilization, enabling Bi NS-L to achieve a formate FE of 94.8 % at −1.08 V *vs.* RHE and a partial current density of 247.5 mA/cm^2 in a flow cell. Moreover, coupling CO_2RR with anodic glycerol oxidation markedly reduced cell voltage, highlighting strain engineering as a promising route for energy-efficient paired electrolysis.

Beyond homogeneous strain modulation, grain boundary engineering can introduce heterogeneous strain fields that further enrich catalytic activity (Fig. 7c) [99]. Under high CO_2 pressure, $BiPO_4$ precursors reconstructed into metallic Bi NSs densely populated with grain boundaries. *Operando* spectroscopy and DFT analyses revealed that these grain boundaries induced local charge redistribution and stabilized HCOO* intermediates, leading to a high formate partial current density of 534 mA/cm^2 and a formation rate of 9.9 mmol h^{-1} cm^{-2} at −0.81 V *vs.* RHE under 3.0 MPa CO_2. These findings collectively demonstrate that strain engineering, from tensile and compressive deformation to grain-boundary-induced heterogeneous strain, provides a powerful toolkit for tuning electronic structure and enhancing CO_2RR efficiency toward industrially relevant conditions.

In addition, the deliberate architectural design of Bi NSs can exploit lattice distortions at specific facets. Micrometer-scale lateral structuring of Bi NSs by cathodic exfoliation introduced tensile strain, narrowing the Bi d-band width and optimizing binding energies for intermediates (Fig. 7d) [100]. The resulting catalysts delivered a record-high mass-normalized partial current density of 590 mA/mg with >90 % selectivity across a broad potential window. Similarly, three-dimensional Bi NSs grown on Cu nanowire cores exhibited preferential exposure of the Bi (110) facet with lattice defects and unsaturated atoms (Fig. 7e) [101]. The synergistic electron transfer from Cu to Bi, combined with facet-induced lattice strain, enhanced the C-terminal hydrogenation of CO_2, achieving >90 % formate selectivity with a current density of 155.8 mA/cm^2.

Finally, the relative contribution of basal and edge planes in strain-tuned activity has been systematically evaluated. By manipulating the orientation of Bi-based precursors, nanosheets with basal-plane dominance exhibited superior CO_2RR performance compared to edge-oriented ones (Fig. 7f) [102]. DFT studies suggested that basal planes effectively suppress competing hydrogen evolution, thereby improving CO_2-to-formate conversion efficiency. This work illustrates how strain effects are facet-dependent, and that optimizing lattice orientation can be as critical as introducing defects or boundaries.

Overall, these studies converge to establish lattice strain, whether compressive, tensile, or grain-boundary induced, as a unifying concept for enhancing Bi nanosheet catalysis. While strain engineering enables extraordinary current densities and selectivities, challenges remain in quantifying strain distributions at the atomic scale and linking them to catalytic performance under *operando* conditions. Advances in strain-resolved spectroscopy, electron microscopy, and multiscale simulations will be indispensable for unraveling these correlations and guiding the rational design of next-generation Bi-based electrocatalysts.

4.3. Doping strategies

Introducing foreign atoms into the bismuth lattice represents one of the most versatile strategies to tune the electronic environment and catalytic activity of Bi NSs. Dopant incorporation alters charge distribution, orbital hybridization, and coordination states, which collectively modulate the adsorption strength of key intermediates (*CO_2^-, *OCHO) and suppress competing hydrogen evolution, thus enabling superior selectivity toward formate/formic acid production [103–105].

Transition-metal incorporation into Bi NSs effectively reshapes their electronic density of states and optimizes orbital overlap with

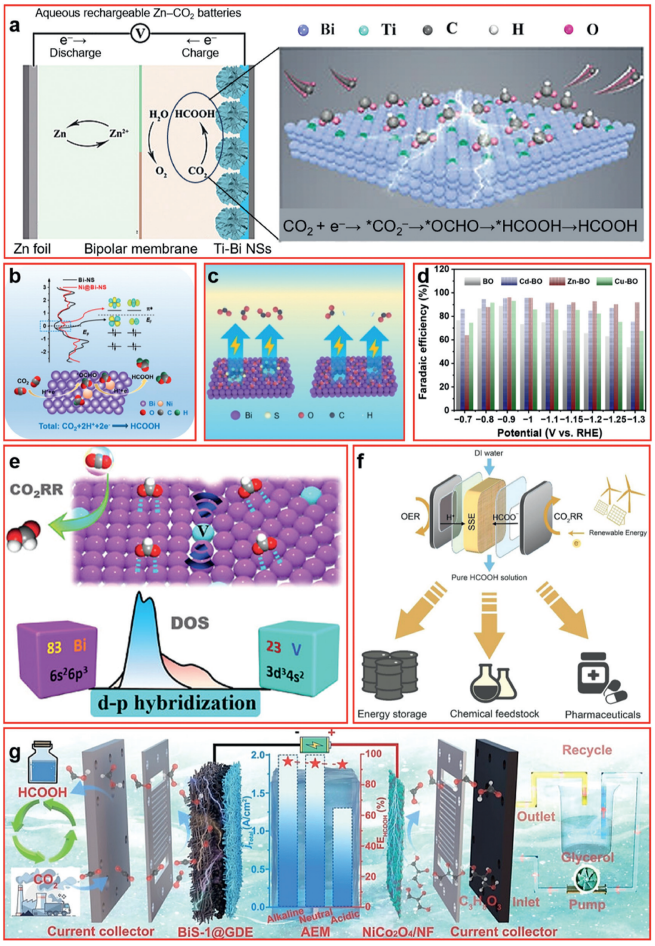


Fig. 8. Doping and electronic modulation strategies in 2D Bi NSs for enhanced CO_2 electroreduction. (a) Ti-doped Bi NSs obtained from electrochemical reduction of $Bi_4Ti_3O_{12}$ combine mass-transfer advantages of ultrathin nanosheets with electron-rich properties of Ti, reaching 96.3 % $FE_{formate}$ and 4032 μmol h^{-1} cm^{-2} production rate at −1.01 V. Reproduced with permission [106]. Copyright 2023, Wiley-VCH. (b) Ni-doped Bi NSs (Ni@Bi-NS) exhibit boosted activity and selectivity toward formate (FE up to 98.4 %) owing to Ni-induced charge transfer that shifts Bi p-orbitals closer to the Fermi level, thereby facilitating *OCHO intermediate formation. Reproduced with permission [107]. Copyright 2022, Wiley-VCH. (c) Sulfur coordination at Bi edge defects effectively passivates H adsorption sites and optimizes charge distribution, leading to enhanced OCHO stabilization and high $FE_{formate}$ ≈95 % at partial current density ≈250 mA/cm^2. Reproduced with permission [108]. Copyright 2023, Wiley-VCH. (d) Zn^{2+} incorporation into Bi_2O_3 nanosheets promotes preferential exposure of (002) facets and stabilizes OCHO intermediates, enabling >90 % $FE_{formate}$ across −0.8∼−1.3 V. Reproduced with permission [109]. Copyright 2023, Springer Nature. (e) Single-atom alloy Bi NSs with *in situ* confined V/Mo/W atoms demonstrate strong p–d orbital hybridization, lowering protonation energy barriers and achieving nearly 100 % selectivity for C_1 products with 90 h stability. Reproduced with permission [110]. Copyright 2024, Wiley-VCH. (f) Co-doped Bi NSs synthesized *via* hydrolysis and operated in a porous solid electrolyte reactor maintain ∼72 % $FE_{formate}$ at 100 mA/cm^2 for 100 h, with DFT indicating lower energy barriers for OCHO stabilization compared to pristine Bi. Reproduced with permission [111]. Copyright 2024, Wiley-VCH. (g) Sulfur-doped BiS-derived catalysts retain partial S after electrochemical reconstruction, delivering record-high $FE_{formate}$ ∼95 % even at ultrahigh current densities (2000 mA/cm^2) across a wide pH range, attributed to S-induced electronic modulation. Reproduced with permission [112]. Copyright 2024, Wiley-VCH.

CO_2 π^* orbitals. Ti-doped Bi NSs, derived from $Bi_4Ti_3O_{12}$ precursors, achieved a formate Faradaic efficiency (FE) of 96.3 % and a current density of 338.3 mA/cm^2, maintaining >90 % selectivity even under demanding operation (Fig. 8a) [106]. Integration into a Zn–CO_2 battery delivered 1.05 mW/cm^2 maximum power density, indicating excellent device compatibility. Similarly, Ni doping shifted the Bi p-band center closer to the Fermi level, enhancing p–π^* hybridization with CO_2 and accelerating *OCHO formation

(Fig. 8b) [107]. Ni–Bi NSs exhibited 98.4 % FE at −0.9 V *vs.* RHE and 2.8-fold higher current density than pristine Bi, demonstrating how transition-metal dopants boost intrinsic reactivity.

Beyond cationic dopants, heteroanion coordination can complement electronic modulation. Sulfur atoms coordinated at Bi edge defects suppressed *H adsorption and optimized *OCHO binding (Fig. 8c) [108]. This cooperative edge–S interaction raised $HCOO^-$ partial currents to ≈ 250 mA/cm^2 with ≈ 95 % selectivity, revealing how targeted anion incorporation simultaneously stabilizes structural edges and enhances activity.

Aliovalent substitution provides a straightforward route to control active surface orientation and electronic structure. Zn^{2+} doping into Bi_2O_3 nanosheets promoted exposure of catalytically active planes, enabling 95 % FE at −0.9 V *vs.* RHE and ≈ 20 mA/cm^2 current density (Fig. 8d) [109]. DFT calculations reveal that Zn substitution stabilizes the OCHO intermediate and lowers the desorption barrier for HCOOH, rationalizing the observed performance enhancement.

Creating single-atom alloys (SAAs) within Bi matrices introduces strong p–d orbital hybridization that redefines adsorption energetics. Incorporating V, Mo, or W atoms into Bi NSs generated grain boundaries and highly delocalized charge density (Fig. 8e) [110]. Among them, Bi–V SAAs achieved nearly 100 % FE for formate from −0.6 V to −1.4 V and remained stable for 90 h. The strong p–d overlap facilitated σ-donation from CO_2 oxygen to Bi sites, lowering the energy barrier for *OCHO protonation and providing a fundamental blueprint for SAA design.

Co doping into Bi NSs further demonstrates the benefits of heteroatom induced electronic reconstruction. Co–Bi NSs prepared by hydrolysis showed superior CO_2RR activity with ∼90 % HCOOH selectivity and 200 mA/cm^2 current density in a porous solid electrolyte cell (Fig. 8f) [111]. *Operando* studies revealed that Co incorporation strengthened *OCHO adsorption and reduced the protonation barrier. Even after 100 h of operation at 100 mA/cm^2, the Co–Bi system retained high selectivity and delivered electrolyte-free HCOOH, underscoring the synergy of activity and durability enabled by transition-metal doping.

Anion-doped precursors can serve as self-reconstructing templates for high-performance CO_2RR. A sulfur-modified bismuth sulfide pre-catalyst (BiS-1) transformed *in situ* into metallic Bi while retaining residual S atoms that modulated the electronic structure (Fig. 8g) [112]. The resulting catalyst exhibited ≈95 % FE across neutral, alkaline, and acidic electrolytes with current densities up to 2000 mA/cm^2 in flow cells and sustained 200 mA/cm^2 for 150 h in a membrane electrode assembly. DFT analysis revealed that residual S atoms promote *HCOO stabilization by lowering the intermediate formation energy, demonstrating how non-metal dopants can be equally decisive in activity control.

Taken together, these advances demonstrate that doping and electronic modulation strategies provide a powerful toolbox for tailoring Bi nanosheet catalysis. Whether through heteroatom substitution, defect–dopant interactions, or orbital hybridization in SAAs, such modifications directly influence the binding energies of CO_2RR intermediates and reaction barriers. While remarkable selectivity (>95 % FE) and industrially relevant current densities (>1 A/cm^2) have been achieved, challenges remain in precisely controlling dopant location, preventing agglomeration at high loadings, and quantifying dopant-induced local electronic effects under *operando* conditions. Addressing these issues will be critical for translating electronic modulation strategies into scalable CO_2RR technologies.

4.4. Mechanistic insights into OCHO intermediate stabilization

The selective stabilization of the OCHO intermediate on Bi-based catalysts has been widely recognized as the decisive step governing both activity and selectivity in CO_2 electroreduction. DFT and *in situ* spectroscopic studies consistently reveal that the adsorption energy and configuration of OCHO are strongly dependent on the local coordination environment, electronic structure, and interfacial microenvironment of Bi active sites.

From a geometric perspective, low-coordination or edge sites significantly reduce the formation barrier of OCHO. Zheng *et al.* demonstrated that edge sites of Bi architectures possess a Gibbs free energy of −0.41 eV for OCHO formation, much lower than that on facet sites (−0.03 eV), rationalizing the superior activity of edge-enriched Bi nanotube assemblies [113]. Similarly, facet engineering enables control over OCHO stabilization: Zhang *et al.* reported that the metastable Bi (101) facet exhibits an exceptionally low OCHO adsorption energy (0.08 eV) compared to the thermodynamically stable Bi (012) facet (0.46 eV), establishing facet-dependent activity–stability correlations [114].

Beyond geometric modulation, electronic regulation through heteroatom doping can tune the p-band center of Bi and thus the binding strength of key intermediates. Ni doping induces charge transfer from Ni to Bi, upshifting the Bi 6p orbital and lowering the energy barrier for OCHO formation from 0.81 eV to 0.69 eV, which accounts for the markedly enhanced formate selectivity [107].

In addition, interfacial and hybrid structures play a vital role in stabilizing OCHO through orbital coupling and charge redistribution. For instance, Zhao *et al.* showed that Bi single-atom intercalation in BiOBr creates a Bi 6p–O 2p orbital hybridization, decreasing the free energy barrier for OCHO formation from 1.30 eV to −0.15 eV and suppressing competing H adsorption [115]. Similarly, Zhang *et al.* constructed $Bi^0/Bi^{\delta+}$–O multi-atomic interfaces that enable selective H–CO_2 coupling and lower the OCHO formation barrier to 0.83 eV [116]. Moreover, the $Bi/Bi_2O_2CO_3$ interfacial phase exhibits moderate adsorption energy (≈0.23 eV) and a low rate-determining barrier (≈0.35 eV) for the $CO_2 \rightarrow$ OCHO step, corroborating the synergistic stabilization at reconstructed Bi/Bi–O interfaces [117].

Finally, microenvironment engineering provides an additional degree of control. Wu *et al.* demonstrated that spatially encoded superhydrophilic–superhydrophobic nanodomains on Bi–PVDF catalysts reorganize interfacial polarity and hydration structure, forming localized dipole fields that selectively stabilize OCHO intermediates and suppress H_2/CO pathways [118].

Collectively, these representative DFT and *operando* findings demonstrate that OCHO stabilization is governed by a concerted interplay between geometric unsaturation, electronic tuning, interface coupling, and microenvironmental regulation. Such multiscale understanding provides a quantitative foundation for the rational design of next-generation Bi-based catalysts with precisely optimized intermediate binding energies and enhanced formate selectivity. Overall, these quantitative insights collectively reveal that OCHO stabilization energy is not an isolated descriptor, but rather an emergent function of atomic coordination, electronic redistribution, interfacial coupling, and local solvation structure—together defining the optimal window of intermediate binding that maximizes both formate selectivity and catalytic durability.

4.5. Interface engineering and hybrid Bi/Bi–O architectures

Engineering interfaces in Bi-based nanostructures has emerged as a powerful strategy to unlock new catalytic functions for the electrochemical CO_2RR. Unlike pristine metallic Bi or stoichiometric oxides, hybrid Bi/Bi–O systems introduce multi-valent states and heterogeneous electronic environments that can stabilize intermediates and suppress competing hydrogen evolution. Moreover, interfacial polarization and synergistic electron transfer endow these systems with remarkable activity and long-term durability under technologically relevant conditions.

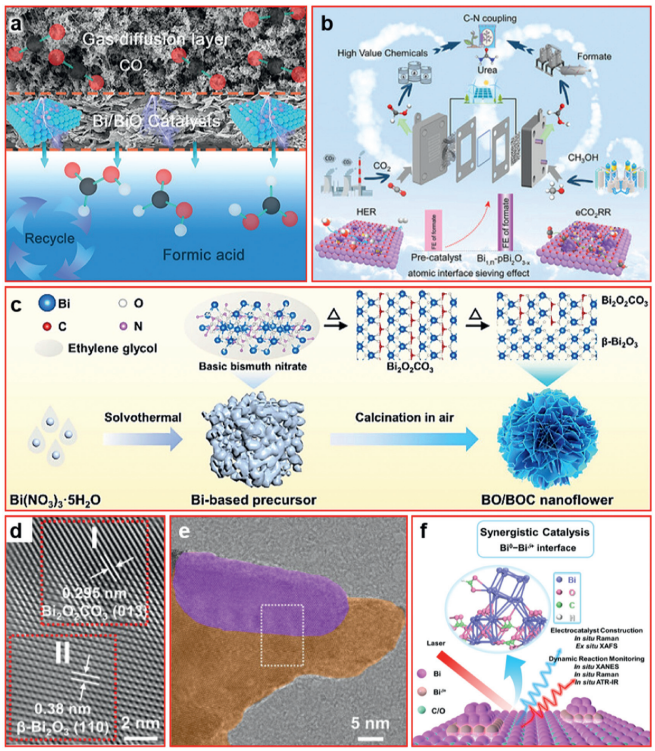


Fig. 9. Interface engineering and hybrid Bi/Bi–O architectures for boosting CO_2 electroreduction performance. (a) MOF-derived leafy Bi NSs with abundant Bi/Bi–O interfacial sites exhibit enhanced CO_2 adsorption and structural stability, achieving FE_{HCOOH} > 90% at current densities exceeding 200 mA/cm^2 in both neutral and alkaline electrolytes, highlighting the role of surface oxygen groups in stabilizing intermediates. Reproduced with permission [119]. Copyright 2020, Wiley-VCH. (b) Porous Bi_2O_{3-x} nanosheets containing multi-atomic $Bi^0/Bi^{\delta+}$–O moieties create an interfacial atomic sieving effect, enabling efficient CO_2-to-formate conversion across pH ranges; moreover, coupling CO_2RR with methanol oxidation allows simultaneous cathodic/anodic formate production for integrated carbon–nitrogen synthesis. Reproduced with permission [116]. Copyright 2025, Wiley-VCH. (c–e) Hybrid β-$Bi_2O_3/Bi_2O_2CO_3$ heterostructures obtained *via* controllable synthesis demonstrate directional electron transfer across the Bi/Bi–O interface, lowering the energy barrier for *OCHO formation and maintaining >94% $FE_{formate}$ over extended operation. Reproduced with permission [120]. Copyright 2025, American Chemical Society. (f) Interface-confined single-atom alloys (V/Mo/W–Bi) with rich grain boundaries establish strong p–d orbital hybridization between Bi and transition-metal dopants, reducing protonation barriers for formate production and delivering nearly 100% Faradaic efficiency for C_1 products over 90 h, while also enabling solar-driven paired catalysis. Reproduced with permission [121]. Copyright 2023, Cell Press.

A representative and scalable route to constructing Bi/Bi–O interfaces is through MOF-derived hybrid nanosheets (Fig. 9a) [119]. In this strategy, leafy Bi NSs obtained from Bi-based MOF precursors expose abundant Bi/Bi–O interfaces while maintaining robust structural integrity under flow-cell conditions. The optimized architecture delivers high current densities (>200 mA/cm^2) and Faradaic efficiencies above 90% for formate over 10 h of continuous operation. *Operando* analyses and DFT calculations further reveal that surface oxygen groups at the Bi/Bi–O boundaries enhance CO_2 adsorption and protect active Bi sites from over-reduction, underscoring the dual protective and activating roles of interfacial oxygen species.

Building upon this concept, deliberate construction of multi-atomic Bi interfaces has emerged as a powerful approach for modulating electronic structure and local coordination environments (Fig. 9b) [116]. Embedding atomically dispersed Bi single atoms and clusters into defect-rich Bi_2O_{3-x} nanosheets generates composite structures with $Bi^0/Bi^{\delta+}$–O moieties. The resulting catalyst achieves an impressive 96.5% Faradaic efficiency for formate at −0.5 V *vs.* RHE across a wide pH range, maintaining stability beyond 150 h. The interfacial "atomic sieving effect" promotes spatially separated adsorption of *H and *CO_2 on distinct sites, enabling selective *OCHO formation while suppressing hydrogen evolution. Moreover, concentrated formate intermediates at the interface facilitate downstream C–N coupling, illustrating how interfacial control can extend CO_2RR toward more complex product pathways.

To further enhance stability, composite $Bi_2O_3/Bi_2O_2CO_3$ heterostructures have been designed to resist over-reduction and structural collapse (Figs. 9c–e) [120]. The coupling of β-Bi_2O_3 with $Bi_2O_2CO_3$ creates a self-buffering alkaline microenvironment that dynamically regenerates Bi–O bonds, thereby maintaining interfacial equilibrium under cathodic potentials. This hybrid structure sustains Faradaic efficiencies above 94% across a wide potential window (−0.7∼−1.1 V) and retains 80% selectivity after 720 h of continuous electrolysis, among the most durable Bi-based CO_2RR systems reported. These results emphasize the critical role of interfacial phase equilibria in achieving long-term catalytic stability.

The intrinsic activity of Bi/Bi–O interfaces has been further clarified through *in situ* and *operando* studies on $Bi/Bi_2O_2CO_3$ thin nanosheets (Bi/BOC TNS) (Fig. 9f) [121]. Spectroscopic and computational analyses revealed that formate generation arises from interfacial charge redistribution: protons generated from water dissociation at metallic Bi^0 sites react with activated CO_2 molecules on neighboring $Bi^{\delta+}$ centers, thereby facilitating *OCHO formation through a synergistic Bi^0–$Bi^{\delta+}$ cooperative mechanism. This work not only identifies the Bi/Bi–O junction as the genuine active site but also highlights the need for advanced *operando* tools to track dynamic interfacial evolution during CO_2RR.

Collectively, these studies demonstrate that Bi/Bi–O hybrid architectures and interface engineering represent a frontier for designing industrially relevant CO_2RR catalysts. Interfacial polarization enables bifunctional catalysis, where metallic sites facilitate proton transfer and reduced oxides stabilize key carbon intermediates. Moreover, controlling dynamic reconstruction through interfacial buffering prevents catalyst collapse, directly addressing the stability challenges of Bi-based materials. Future research should focus on quantifying the interplay between local coordination, defect density, and interfacial electronic structures under *operando* conditions. Such efforts will pave the way toward rationally engineered interfaces that combine activity, selectivity, and durability at scale.

4.6. Synergistic engineering with conductive supports and heterostructures

While Bi NSs exhibit excellent intrinsic selectivity toward formate, their activity is often limited by insufficient conductivity, sluggish CO_2 adsorption, and structural instability. To overcome these limitations, recent studies have highlighted the effectiveness of coupling Bi NSs with conductive supports and transition-metal oxides (TMOs), thereby creating synergistic heterostructures that optimize charge transport, enhance CO_2 activation, and stabilize active intermediates [122].

A representative example is the integration of transition-metal oxides (TMOs) with metallic Bi NSs (Fig. 10a) [123]. By introducing Fe_2O_3, Co_3O_4, or NiO onto Bi NSs, strong interfacial orbital interactions between Bi p and transition-metal d states were established. *In situ* Fourier-transform infrared spectroscopy and CO_2-TPD analyses revealed that these heterostructures enhanced CO_2 adsorption and stabilized the *OCHO intermediate. DFT calculations further showed that orbital modulation reduced the overpotential for both *CO_2-to-*OCHO conversion and subsequent *OCHO-to-HCOOH desorption. Among them, Bi/Fe_2O_3 NSs delivered the most significant improvement, achieving a maximum Faradaic efficiency (FE) of 99.7% for formate with a partial current density of

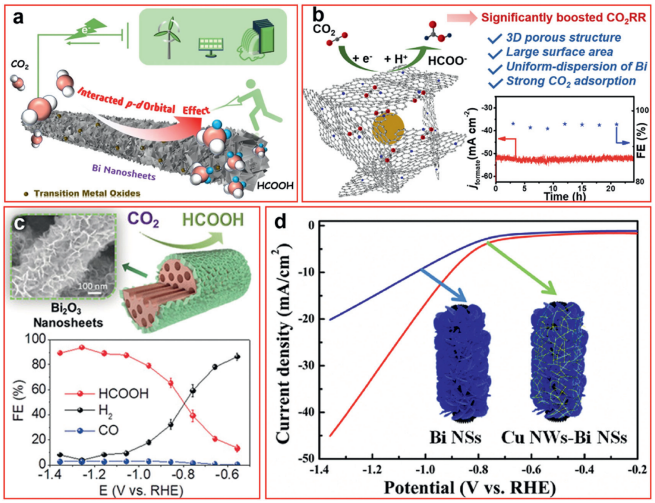


Fig. 10. Synergistic engineering of conductive supports and heterostructures for enhanced CO_2 electroreduction on Bi-based nanosheets. (a) Transition-metal oxide (TMO)–modified Bi NSs (Bi/TMO NSs) establish synergistic p–d orbital interactions between Bi and TMOs, lowering the energy barrier for *OCHO formation and electron transfer. Among them, Bi/Fe_2O_3 NSs achieve nearly 99.7% FE_{HCOOH} at −0.8 V *vs.* RHE, outperforming pristine Bi. Reproduced with permission [123]. Copyright 2024, Science China Press. (b) Nitrogen-doped graphene aerogel (NGA) matrices coupled with Bi nanoplates enhance strong metal–support interactions, increase surface area, and regulate interfacial wettability, thereby achieving FE_{HCOOH} of 96.4% at 51.4 mA/cm^2 in aqueous electrolyte. Reproduced with permission [124]. Copyright 2023, American Chemical Society. (c) Hierarchical Bi_2O_3 nanosheets grown on a conductive multiple-channel carbon matrix (MCCM) exhibit FE_{HCOOH} up to 93.8% and superior energy efficiency, where MCCM accelerates electron transfer and CO_2 adsorption while ultrathin Bi_2O_3 nanosheets provide abundant exposed active sites. Reproduced with permission [125]. Copyright 2019, Wiley-VCH. (d) Cu nanowire–bridged Bi NSs arrays on carbon cloth (Cu NWs–Bi NSs) demonstrate higher current density and selectivity than pristine Bi, benefiting from the electronic modulation and charge transfer facilitated by conductive Cu NWs. Reproduced with permission [126]. Copyright 2020, Elsevier.

12.65 mA/cm^2 at −0.8 V *vs.* RHE. This study establishes p–d orbital coupling as a versatile approach to enhance the thermodynamics and kinetics of Bi-catalyzed CO_2RR.

Beyond oxide coupling, carbon-based conductive matrices provide another route to address the limitations of Bi NSs. Embedding Bi nanoplates in a three-dimensional nitrogen-doped graphene aerogel (NGA) (Fig. 10b) [124] not only increased the accessible surface area but also introduced strong metal–support interactions (SMSI). The porous aerogel regulated local wettability and facilitated mass transfer, while nitrogen functionalities in the graphene skeleton strengthened CO_2 adsorption. As a result, Bi/NGA composites achieved a high formate FE of 96.4% with a current density of 51.4 mA/cm^2 at −1.0 V *vs.* RHE, outperforming pristine Bi. Similarly, constructing hierarchical architectures by growing Bi_2O_3 nanosheets on a multi-channel carbon matrix (MCCM) (Fig. 10c) [125] offered a dual advantage of fast electron transfer through the conductive carbon framework and abundant active sites provided by ultrathin Bi_2O_3 layers. The resulting hybrid catalyst reached a FE of 93.8% with an energy efficiency of 55.3% and demonstrated stable operation over 12 h, highlighting the critical role of host–guest synergy in stabilizing high-surface-area Bi architectures.

In addition to carbon supports, metallic scaffolds such as Cu nanowires (Cu NWs) have been explored to improve charge transfer and electronic coupling with Bi NSs. Cu NW–bridged Bi nanosheet arrays (Fig. 10d) [126] demonstrated superior activity compared to pristine Bi, owing to the partial electron donation from Cu to Bi that enhanced Bi reducibility and stabilized CO_2 reduction intermediates. This interfacial charge redistribution led to higher current densities and improved formate selectivity, further corroborating the promise of metallic heterostructures as conductive platforms.

Taken together, these studies highlight that synergistic engineering with conductive supports and heterostructures addresses the intrinsic limitations of Bi NSs by simultaneously improving electronic conductivity, optimizing adsorption energetics, and facilitating mass/electron transport. Importantly, these strategies not only improve performance metrics such as current density and Faradaic efficiency but also extend catalyst lifetimes, moving Bi-based CO_2RR catalysts closer to industrial application. Future directions include rationally tuning the degree of metal–support interaction, integrating multi-functional supports (*e.g.,* dual-conductive and ion-conductive frameworks), and employing *operando* characterization to unravel the dynamic evolution of these heterostructures under high-current operation.

4.7. In situ reconstruction and dynamic evolution of Bi-based catalysts

An emerging paradigm in Bi-based CO_2 electroreduction catalysis is that the real active sites often differ significantly from the pristine precursors due to inevitable reconstruction under electrochemical conditions. Rather than being detrimental, such *in situ* structural evolution can generate highly active and selective catalytic phases, particularly when it is deliberately controlled and harnessed [127].

Controlled *in situ* reduction of $Bi(OH)_3$ precursors produces ultrathin Bi NSs enriched with coordinatively unsaturated pit sites (Fig. 11a) [128]. These defective regions serve as highly active centers for *OCHO stabilization, enabling current densities up to 325 mA/cm^2 without compromising selectivity. This example highlights how rationally induced reconstruction can maximize the density of catalytically accessible Bi sites.

Bi-based metal–organic frameworks (MOFs) have proven to be versatile precursors for generating oxide-derived Bi catalysts *via* sequential reconstruction steps (Figs. 11b and c) [129,130]. During CO_2RR, HCO_3^- ions selectively cleave Bi–O bonds, transforming the MOF columns into ultrathin $Bi_2O_2CO_3$ sheets with favorable surface energetics for *OCHO adsorption [129]. Upon further cathodic reduction, these sheets convert to metallic Bi while retaining abundant unsaturated Bi sites that act as the true active centers [130]. Such electrolyte- and potential-driven multistep reconstruction offers a controllable route to achieve catalysts with both high activity and durability.

Reversible reconstruction can also underpin exceptional long-term durability. In $Bi_{0.6}Cu_{0.4}$ nanosheets, cyclic voltammetry treatments continuously regenerated catalytically active Bi–O motifs, maintaining > 90% Faradaic efficiency for formate over 400 h at 260 mA/cm^2 (Fig. 11d) [131]. *Operando* Raman spectroscopy revealed the dynamic reappearance of Bi–O vibrations, revealing that reversible Bi–O reformation sustains catalytic selectivity and efficiency under industrial current densities.

The surrounding chemical environment exerts decisive control over reconstruction dynamics. When BiOCOOH nanowires were reduced in CO_2-saturated electrolyte, they evolved into ultrathin Bi/BiO_x nanosheets with enhanced CO_2 adsorption and charge transfer properties. In contrast, reduction in Ar-saturated HCOONa solution produced unstable Bi nanowires prone to fragmentation (Fig. 11e) [132]. These results emphasize that electrolyte composition governs both phase evolution and final catalytic architecture.

Low-crystallinity Bi oxyhalide precursors undergo rapid electrochemical reduction into lattice-distorted Bi NSs with compressive strain (Fig. 11f) [97]. Such compressive distortion promotes CO_2 adsorption and stabilizes *OCHO intermediates, delivering 94.8% FE and 247 mA/cm^2 partial current density—significantly outperform-

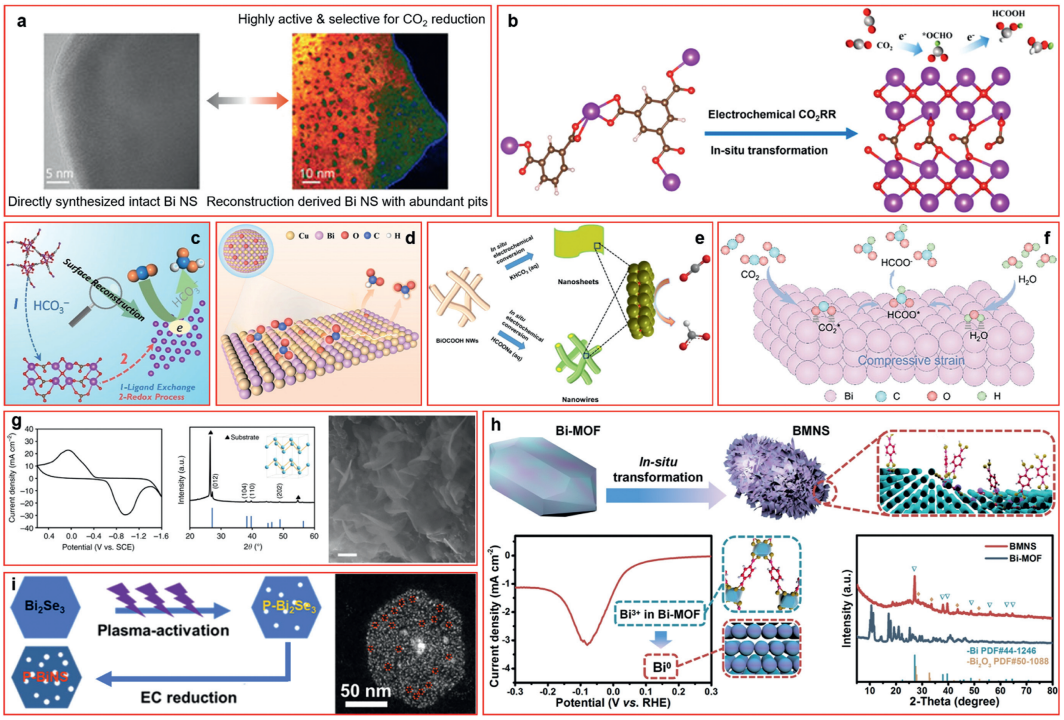


Fig. 11. *In situ* reconstruction and dynamic evolution of Bi-based catalysts during electrochemical CO_2 reduction. (a) *In situ* structural reconstruction of $Bi(OH)_3$ nanosheets generates coordinatively unsaturated pit sites on Bi NSs, which act as the real active centers, achieving >95 % FE_{HCOO^-} and industrial-level current density of 325 mA/cm^2 in flow cells. Reproduced with permission [128]. Copyright 2022, Wiley-VCH. (b) Microwave-assisted Bi-BTC MOF evolves into $Bi_2O_2CO_3$ nanosheets during CO_2RR, with the restructured phase lowering the energy barrier for *OCHO stabilization, thereby delivering 96 % $FE_{formate}$ at −0.9 V. Reproduced with permission [129]. Copyright 2024, American Chemical Society. (c) A two-step reconstruction of Bi-MOF—electrolyte-mediated dissociation to $Bi_2O_2CO_3$, followed by potential-driven reduction to metallic Bi—creates unsaturated Bi active sites, enabling excellent selectivity and stability for formate generation. Reproduced with permission [130]. Copyright 2021, Wiley-VCH. (d) Cyclic voltammetry–induced reconstruction of $Bi_{0.6}Cu_{0.4}$ nanosheets regenerates Bi–O moieties, maintaining >90 % FE_{HCOO^-} for over 400 h at 260 mA/cm^2, representing one of the longest stability reports at industrial current density. Reproduced with permission [131]. Copyright 2023, Springer Nature. (e) Electrolyte-dependent evolution of BiOCOOH nanowires leads to Bi/BiOx nanosheets with superior activity and durability compared to porous Bi nanowires, due to enhanced CO_2 adsorption and charge transfer across the amorphous oxide shell. Reproduced with permission [132]. Copyright 2023, Springer Nature. (f) Crystallinity-mediated reconstruction reveals that low-crystalline BOC precursors form lattice-compressive Bi NSs with superior activity (94.8 % $FE_{formate}$ at −1.08 V), while high-crystalline counterparts yield less active ordered Bi phases. Reproduced with permission [97]. Copyright 2025, American Chemical Society. (g) Topotactic reduction of BiOI produces metallic Bi NSs with ordered crystal domains, as evidenced by CV, XRD, SEM, TEM, and SAED characterizations. Reproduced with permission [67]. Copyright 2018, Springer Nature. (h) Ligand-stabilized Bi NSs (BMNS) are reconstructed from Bi-MOF precursors, where residual ligands help redistribute Bi atoms and stabilize under-coordinated active sites. Reproduced with permission [91]. Copyright 2021, Elsevier. (i) Schematic illustration of the evolution from pre-catalyst Bi_2Se_3 nanosheets to plasma-activated P-Bi_2Se_3 and subsequently to the final P-BiNS catalyst, accompanied by the corresponding STEM image. Reproduced with permission [46]. Copyright 2024, Elsevier.

ing high-crystallinity analogues. This demonstrates that precursor crystallinity can be exploited to regulate strain fields and intrinsic catalytic activity.

Beyond crystallinity control, topotactic conversion of BiOI into ultrathin Bi NSs yields highly ordered, single-crystalline nanosheets with large surface area and nearly 100 % formate selectivity across broad potentials (Fig. 11g) [67]. These 2D structures exhibit excellent durability and are compatible with device integration, underscoring the practical benefits of halide-derived topotactic reconstruction. *In situ* reduction of Bi–MOF precursors can also preserve under-coordinated Bi sites through ligand stabilization (Fig. 11h) [91]. Residual organic ligands prevent particle agglomeration while maintaining abundant surface Bi atoms, yielding ≈ 98 % FE for formate with prolonged lifetime. This demonstrates that controlled retention of ligand environments can effectively stabilize reconstructed Bi NSs.

Plasma-induced reconstruction provides a rapid and versatile route to generate ultrathin, defect-rich Bi NSs (P-BiNS) from layered Bi_2Se_3 (Fig. 11i) [46]. The plasma activation enlarges the surface area, increases active-site density, and stabilizes *OCHO intermediates, achieving >90 % FE at >80 mA/cm^2 and stable operation for >50 h. DFT analyses attribute this performance to favorable charge redistribution and intermediate binding on the P-BiNS surface, validating plasma-enabled reconstruction as a scalable catalyst design route.

Taken together, these advances establish that reconstruction is not a side-effect but a design principle in Bi-based CO_2RR catalysis. By tailoring precursor crystallinity, exploiting MOF or oxyformate scaffolds, stabilizing unsaturated Bi *via* ligand or oxide anchoring, and dynamically regenerating Bi–O motifs under operation, researchers have achieved catalysts that combine high activity, exceptional selectivity, and industrial-level durability. Future work should focus on *operando* multi-scale tracking of reconstruction, as well as predictive control of phase transformations, to fully leverage dynamic evolution as a robust strategy for practical CO_2 electroreduction.

4.8. Microenvironment and reaction condition engineering

The catalytic performance of Bi-based nanosheets in CO_2 electroreduction is not only determined by their intrinsic structure, but is also profoundly influenced by the surrounding electrochemical microenvironment and external reaction conditions. Rationally tuning factors such as local pH, electrolyte composition, and reaction cell configuration has proven to be a powerful strategy to simultaneously optimize selectivity, activity, and durability.

One major challenge for Bi-based catalysts lies in uncontrolled reduction reconstruction, which can cause the collapse of well-defined structures and consequent deactivation under working conditions. A recent study demonstrated that constructing a β-

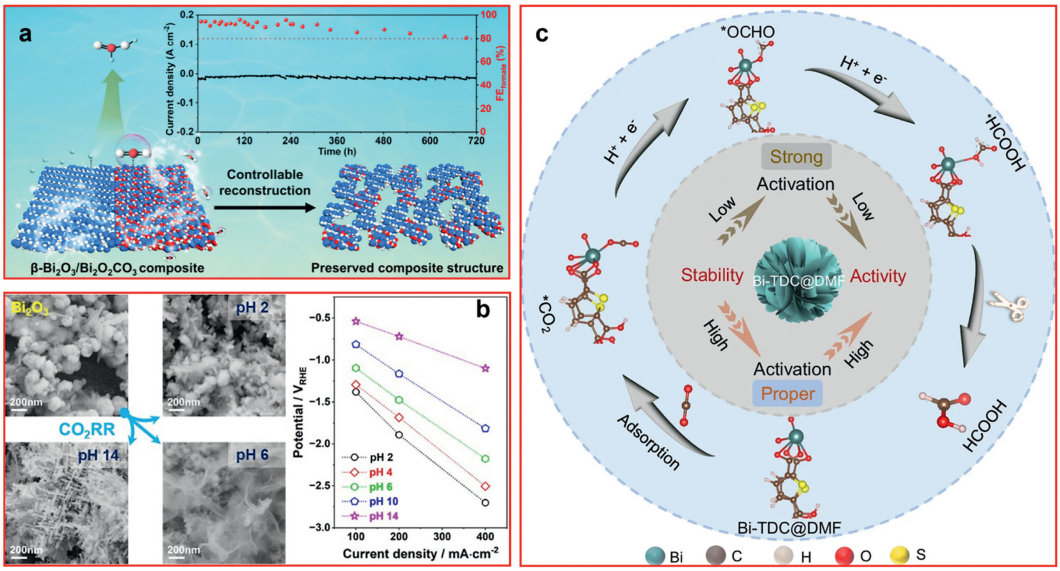


Fig. 12. Engineering the reaction microenvironment and operation conditions to enhance the performance of Bi-based catalysts in electrochemical CO_2 reduction. (a) Construction of a β-Bi_2O_3/$Bi_2O_2CO_3$ composite that resists uncontrolled electrochemical reconstruction to metallic Bi by modulating a locally alkaline microenvironment. The stable heterointerface promotes directional electron transfer and sustained Bi–O bonding, delivering >94 % $FE_{formate}$ over −0.7∼ −1.1 V and maintaining 80 % selectivity after 720 h of continuous operation. Reproduced with permission [120]. Copyright 2025, American Chemical Society. (b) Bi_2O_3 gas diffusion electrodes (Bi-GDEs) synthesized *via* a microwave-assisted process show near-unit selectivity (>95 % $FE_{formate}$) across a wide pH range. *Operando* Raman spectroscopy and post-mortem SEM reveal that electrolyte pH governs structural evolution, while highly alkaline conditions induce dendritic morphologies with doubled electrochemical surface area, thus enhancing current density and catalytic activity. Reproduced with permission [133]. Copyright 2025, The Chemical Society of Japan. (c) Schematic diagram of Bi-TDC@DMF-catalyzed CO_2RR, highlighting the activity–stability trade-off during formate production, where optimized local coordination and reaction conditions balance efficiency and durability. Reproduced with permission [134]. Copyright 2024, Springer Nature.

Bi_2O_3/$Bi_2O_2CO_3$ composite could effectively resist over-reduction by stabilizing new Bi–O bonds in a locally alkaline microenvironment (Fig. 12a) [120]. The cooperative interaction between the β-Bi_2O_3 and $Bi_2O_2CO_3$ domains not only provided directional electron transfer pathways but also maintained structural integrity over extended operation. As a result, the composite achieved Faradaic efficiencies above 94 % across a wide potential range and retained 80 % selectivity even after 720 h of continuous electrolysis, setting a new benchmark for catalyst durability. This work underscores how engineered microenvironments can protect active phases from collapse and extend catalyst lifetime in industrially relevant conditions.

Beyond stability, the electrolyte pH has been identified as a decisive factor in dictating both activity and structural evolution of Bi_2O_3 nanostructures (Fig. 12b) [133]. *Operando* Raman spectroscopy and post-mortem analyses revealed that Bi_2O_3 more readily reduces under highly acidic or basic conditions, whereas near-neutral pH slows down the reduction process. Despite these structural variations, metallic Bi consistently emerges as the active phase, explaining the nearly universal selectivity toward formate observed across diverse electrolytes. Interestingly, under highly alkaline conditions (pH 14), Bi_2O_3 develops hierarchical dendritic structures with doubled double-layer capacitance, reflecting a significant increase in electrochemically active surface area. These results highlight that reaction medium–induced reconstruction can be harnessed to tune surface area and activity, although precise control remains necessary to balance performance and structural robustness.

A frontier direction involves extending Bi-based CO_2 electroreduction into acidic media, where competing hydrogen evolution, corrosion, and product crossover typically suppress formate selectivity. Leveraging Pourbaix diagram-guided design, an acid-tolerant Bi-MOF was recently employed in a proton-exchange-membrane electrolyzer (Fig. 12c) [134]. This system delivered industrially relevant current densities (250–400 mA/cm^2) with Faradaic efficiencies above 93 % for formic acid, while maintaining stability over 100 h. Notably, the process achieved a high single-pass CO_2 conversion efficiency (64.9 %) and energy consumption as low as 200.65 kWh/kmol, indicating clear advantages for scaling towards commercial implementation. Such advances demonstrate that device-level engineering combined with catalyst microenvironment design can overcome long-standing limitations in acidic CO_2 electrolysis.

In conclusion to this section, engineering the local microenvironment, whether through composite-induced alkalinity, pH-dependent morphological regulation, or acid-tolerant MOF architectures in advanced electrolyzer designs, offers a versatile toolkit to enhance the overall catalytic performance of Bi-based nanosheets. Future work should focus on *operando* multiparameter control, coupling electrolyte design with catalyst architecture and cell engineering, to establish robust, scalable, and energy-efficient CO_2RR platforms.

Following the discussion of individual regulatory strategies, the collective insights from Section 4 can be integrated into a unified mechanistic framework for understanding and optimizing 2D Bi NSs in CO_2 electroreduction. From the atomic to the device level, the seven interrelated design approaches, defect engineering, lattice strain modulation, heteroatom doping, interface construction, conductive support coupling, dynamic reconstruction, and microenvironment regulation, work synergistically to tune the local coordination, electronic configuration, and reaction environment of Bi active sites. Mechanistically, defect creation and strain modulation expose unsaturated Bi sites and adjust orbital overlap, facilitating CO_2 activation and OCHO intermediate stabilization. Doping and interface engineering further redistribute charge and optimize orbital hybridization, selectively promoting proton–electron transfer while suppressing competing hydrogen evolution. Integration with conductive or hybrid supports ensures efficient charge and mass transport, whereas controlled *in situ* reconstruction dynamically regenerates active Bi phases and enhances operational

durability. Finally, microenvironment tailoring, including electrolyte and pH optimization, fine-tunes local ion transport and potential gradients, bridging the gap between intrinsic catalytic activity and device-level efficiency. Collectively, these interlinked strategies reveal that structural and electronic regulation in 2D Bi NSs is not a series of isolated modifications but a mutually reinforcing, hierarchical design paradigm. This holistic understanding establishes the conceptual foundation for rationally engineering next-generation Bi-based catalysts that combine high selectivity, industrial-level current densities, and long-term durability for sustainable CO_2-to-formate conversion.

5. Overall summary of current advances

Building upon the mechanistic framework established in Section 4, which integrates structural and electronic regulation strategies for optimizing 2D Bi NSs in CO_2 electroreduction, this section provides an overarching summary of the current advances in the field.

Over the past decade, the exploration of two-dimensional (2D) Bi NSs has undergone remarkable progress, from the development of controllable synthesis strategies to their deployment in electrocatalytic CO_2RR. The advances summarized in this review highlight three interconnected aspects, synthetic methodology, structure–property relationships, and catalytic mechanisms, which collectively delineate the current status of this rapidly evolving field.

5.1. Advances in synthesis

Multiple routes have been developed to prepare 2D Bi NSs with tailored morphology and surface chemistry. Bottom-up chemical reduction and electrochemical deposition offer scalable access to ultrathin nanosheets with abundant exposed active sites. Top-down exfoliation enables the acquisition of single- or few-layer Bi with preserved crystallinity and well-defined basal planes. Meanwhile, physical vapor deposition and thermal methods provide high structural precision and allow integration with conductive supports. These diverse approaches have created a versatile toolbox to tune the thickness, surface states, and defect density of Bi NSs, which are essential determinants of their catalytic behavior.

5.2. Application strategies for CO_2RR

Recent efforts have extended beyond simple utilization of pristine Bi NSs to engineering more sophisticated catalytic environments. Defect and vacancy engineering facilitates the formation of unsaturated coordination sites that strengthen CO_2 activation. Lattice distortion and strain modulation provide electronic flexibility, enhancing *OCHO intermediate stabilization. Heteroatom doping and electronic modulation further enrich the electronic landscape, enabling fine control over adsorption energetics. Interface design—particularly Bi/Bi–O hybrids—optimizes charge redistribution and promotes selective proton–electron transfer. In parallel, synergistic coupling with conductive scaffolds effectively improves charge/mass transport, while dynamic *in situ* reconstruction of Bi oxides, hydroxides, and metal–organic precursors uncovers catalytically active states that are inaccessible in pristine phases. Finally, microenvironment engineering through electrolyte regulation or membrane reactors provides an additional lever to suppress hydrogen evolution and extend catalytic durability under industrially relevant current densities. Collectively, these strategies represent a comprehensive framework to maximize the intrinsic activity of Bi NSs while ensuring structural resilience.

5.3. Mechanistic understanding

The accumulation of experimental evidence and DFT calculations has significantly advanced our understanding of CO_2RR pathways on Bi NSs. *In situ* and *operando* spectroscopic studies, including Raman, ATR-IR, and X-ray absorption, have identified *OCHO as the key intermediate and revealed its stabilization by low-coordinated Bi sites, orbital hybridization, and interfacial charge polarization. At the same time, *operando* monitoring has revealed the dynamic structural evolution of Bi-based pre-catalysts, emphasizing that the "real" active states often differ from the initial structures. These mechanistic insights establish clear correlations between synthetic control, structural evolution, and catalytic performance, laying the groundwork for rational catalyst design.

In summary, current research has demonstrated that 2D Bi NSs are not only highly selective toward formate/formic acid production but also capable of operating at industrially relevant current densities with extended stability. The integration of synthetic innovation, strategic catalytic engineering, and mechanistic elucidation has propelled this field from fundamental feasibility studies toward practical relevance. Nevertheless, challenges remain in reconciling activity with long-term stability, achieving scalable synthesis with atomic precision, and bridging mechanistic insights to device-level performance. These challenges, along with emerging opportunities, will be critically discussed in the following section on future perspectives.

6. Perspectives and future directions

The rapid progress in the synthesis and application of two-dimensional (2D) Bi NSs for CO_2 electroreduction has firmly established them as one of the most promising catalyst families for selective formate production. However, despite notable achievements, several scientific and technological hurdles remain before these materials can be reliably translated into industrial-scale electrolysis. Looking forward, we identify several key research directions that merit particular attention.

6.1. Precise structural control at the atomic scale

Although bottom-up and top-down routes have enabled synthesis of Bi NSs with tunable thickness, crystallinity, and surface states, achieving atomic-level precision across large areas remains a challenge. Future research should focus on scalable synthesis protocols that combine atomic precision with reproducibility. *In situ* monitoring techniques, such as *operando* TEM and synchrotron-based X-ray absorption, could provide real-time feedback to guide the growth of defect-engineered or doped Bi NSs with deterministic structures.

6.2. Understanding and controlling dynamic reconstruction

Increasing evidence indicates that the "true" active phase of Bi-based catalysts often emerges through electrochemical reconstruction. While this dynamic evolution can create highly active unsaturated sites, it also introduces uncertainty in catalyst durability. Moving forward, quantitative control over reconstruction pathways, for example, through electrolyte engineering, potential programming, or predesigned heterostructures, will be critical. Developing regenerable catalysts that maintain structural integrity under high current densities is another promising direction.

6.3. Integrative design of multi-scale architectures

Single nanosheets, though highly active, are insufficient to address challenges of mass transport and current distribution at device scale. Hierarchical electrode architectures that integrate 2D

Bi NSs into conductive 3D scaffolds or porous flow-cell electrodes could bridge the gap between nanoscale activity and macroscale performance. Rational coupling with conductive carbon networks, nanowires, or ionomer coatings should be pursued to enhance electron delivery, gas diffusion, and electrolyte management simultaneously.

6.4. Expanding the scope of product selectivity

Currently, most Bi NS catalysts show near-unity selectivity toward formate. While this is advantageous for single-product systems, exploring reaction pathways toward higher-value C–C coupled products or integrated co-electrolysis remains underexplored. For example, coupling CO_2 reduction with anodic biomass oxidation or with N-containing species for urea or carbamate formation may open new avenues for circular carbon–nitrogen utilization. Designing Bi-based catalysts that selectively stabilize intermediates beyond *OCHO could significantly broaden their applicability.

6.5. Device integration and operational stability

Translating laboratory-scale performance into practical electrolysis systems requires overcoming additional barriers, including long-term stability under fluctuating current densities, resistance to electrolyte flooding, and compatibility with membrane electrode assemblies (MEAs). Integrating Bi NSs into solid electrolyte reactors or proton exchange membrane systems, while mitigating acid corrosion and hydrogen evolution, will be essential for commercial relevance. Future studies should report standardized benchmarking metrics, such as energy efficiency, single-pass conversion, and product concentration, to allow direct comparison with competing catalyst systems.

6.6. Data-driven and theory-guided discovery

Finally, the integration of machine learning, high-throughput computation, and automated experimentation offers a promising route to accelerate discovery. Data-driven frameworks could help identify hidden descriptors correlating Bi NSs' structural motifs with catalytic outcomes, thereby enabling rational screening of dopants, defects, or hybrid architectures. When combined with *operando* characterization, such approaches could transform empirical optimization into predictive design.

6.7. Outlook

In summary, 2D Bi NSs have reached a pivotal stage where their intrinsic catalytic advantages are well recognized, yet their practical deployment depends on tackling remaining synthesis, mechanistic, and device-level challenges. Future advances will likely arise from synergistic efforts across materials chemistry, *in situ* spectroscopy, computational modeling, and electrochemical engineering. With continued interdisciplinary progress, Bi NS-based catalysts may evolve from model systems for fundamental CO_2RR studies into technologically viable platforms for sustainable formate production and beyond.

Declaration of competing interest

The authors declare that they have no known competing financial interests or personal relationships that could have appeared to influence the work reported in this paper.

CRediT authorship contribution statement

Chuncheng Xu: Writing – original draft. **Suqin Han:** Writing – original draft. **Kaiyang Zhang:** Writing – original draft, Visualization, Conceptualization. **Qiuling Feng:** Visualization. **Lan Bao:** Investigation. **Mingming Gao:** Investigation. **Wen-Yan Gao:** Investigation, Methodology, Supervision. **Yen Leng Pak:** Funding acquisition. **Hongyu Mou:** Supervision. **Liwei Chen:** Writing – review & editing, Funding acquisition. **Xing Gao:** Supervision. **Yuchen Hao:** Writing – review & editing, Supervision, Funding acquisition.

Acknowledgments

This work is supported by the Shandong Provincial Natural Science Foundation (Nos. ZR2024QB122, ZR2024QE448), Research Program of Qilu Institute of Technology (No. QIT23TP011), National Key Research and Development Program of China (No. 2020YFB1506300), National Natural Science Foundation of China (Nos. 22405069, 82202240), the Taishan Scholar Young Talent Program (No. tsqn202211249). The authors would like to thank Shiyanjia Lab (www.shiyanjia.com) for the language editing service.

References

[1] R. Li, Y. Li, P. Yang, et al., J. Energy Chem. 57 (2021) 547–566.
[2] H. Zheng, Z. Yang, L. Luo, et al., Nano Lett. 25 (2025) 8750–8757.
[3] Y. Luo, S. Chen, J. Zhang, et al., Adv. Mater. 35 (2023) 2303297.
[4] Z. Li, B. Sun, D. Xiao, et al., Angew. Chem. Int. Ed. 11 (2023) e202217569.
[5] Y. Wang, S. Xia, R. Cai, et al., Angew. Chem. Int. Ed. 16 (2024) e202318589.
[6] Y. Sheng, Y. Guo, H. Yu, et al., Small 16 (2023) 2207305.
[7] X. Teng, K. Shi, L. Chen, J. Shi, Angew. Chem. Int. Ed. 7 (2024) e202318585.
[8] L. Ding, Y. Ding, F. Bai, et al., Inorg. Chem. 62 (2023) 2289–2303.
[9] L. Liu, J. Hu, Z. Ma, et al., Nat. Commun. 15 (2024) 305.
[10] Q. Zhang, C. Zhang, H. Wang, et al., Fuel 403 (2026) 136111.
[11] C. Dong, H. Song, L. Bu, et al., Nano Lett. 25 (2025) 12285–12293.
[12] W. Dai, J. Long, L. Yang, et al., J. Energy Chem. 61 (2021) 281–289.
[13] D. Wen, J. Zhao, Y. You, et al., Energy Environ. Sci. 17 (2024) 6245–6255.
[14] F. Bienen, A. Löwe, J. Hildebrand, et al., J. Energy Chem. 62 (2021) 367–376.
[15] H. Ren, X. Wang, X. Zhou, et al., J. Energy Chem. 79 (2023) 263–271.
[16] T. Wissink, A.J.W. Man, W. Chen, et al., J. CO_2 Util. 77 (2023) 102604.
[17] C. Jiang, S. Zeng, J. Feng, et al., J. Mater. Chem. A 12 (2024) 14809–14815.
[18] L. Ding, Y. Li, Y. Ding, et al., Appl. Surf. Sci. 624 (2023) 157100.
[19] G. Sun, C. Zou, W. Sun, et al., Mater. Chem. Front. 7 (2023) 3382–3389.
[20] L. Zhang, T. Wang, X. Zhang, P. Dub, ACS Sustain. Chem. Eng. 12 (2024) 14070–14076.
[21] Y.X. Feng, G.X. Dong, K. Su, et al., J. Energy Chem. 69 (2022) 348–355.
[22] Z. Tan, J. Zhang, Y. Yang, et al., CCS Chem. 6 (2024) 100–109.
[23] M. Guan, N. Lu, X. Zhang, et al., Carbon Energy 4 (2024) e420.
[24] Z.H. Zhu, Z.L. Liang, S.L. Hou, et al., J. Energy Chem. 63 (2021) 328–335.
[25] X. Liu, K. Li, L. Cheng, et al., ChemCatChem 8 (2025) e202402151.
[26] J. Tu, J. Li, Z. Pan, et al., J. Power Sources 624 (2024) 235618.
[27] Y. Pang, R. Xie, H. Xie, et al., ACS Appl. Nano Mater. 16 (2024) 42109–42117.
[28] T. Sun, K. Wang, Y. Du, et al., Appl. Catal. B 381 (2026) 125849.
[29] H. Wei, Z. Li, H. Wang, et al., J. Energy Chem. 82 (2023) 18–24.
[30] Y. Li, J. Chen, S. Chen, et al., Appl. Catal. B 349 (2024) 123874.
[31] P. Lei, S. Liu, Q. Wen, et al., Angew. Chem. Int. Ed. 3 (2025) e202415726.
[32] H. Ding, H. Wu, J. Ma, et al., Sep. Purif. Technol. 354 (2025) 129305.
[33] L. Zhao, H. Hou, S. Wang, et al., Adv. Funct. Mater. 9 (2025) 2416346.
[34] Y. Liu, S. Zhao, J. Zhong, et al., Sci. China Mater. 67 (2024) 3609–3621.
[35] Y. Wang, W. Chen, Y. Li, J. Colloid. Interf. Sci. 686 (2025) 1168–1174.
[36] C. Peng, S. Yang, G. Luo, et al., Chem 9 (2023) 2830–2840.
[37] M. Cheng, B. Gao, X. Zheng, et al., Appl. Catal. B 353 (2024) 124097.
[38] D. Lai, M. Xie, H. Zhao, et al., Electrochim. Acta 464 (2023) 142893.
[39] J. Zhu, Y. Tong, H. Xu, et al., ACS Sustain. Chem. Eng. 12 (2024) 938–946.
[40] Y. Xie, C. Wang, Y. Chen, et al., J. Environ. Sci. 150 (2025) 267–276.
[41] W. Chen, R. Chen, Y. Jiang, et al., Small 11 (2024) 2306795.
[42] Y. Zhou, J. Jiang, H. Yin, S. Zhang, Dalton Trans. 53 (2024) 16066–16075.
[43] S. Zhao, Y. Qin, X. Wang, et al., Small 43 (2023) 2302878.
[44] D. He, G. Huang, J. Hu, et al., Adv. Energy Mater. 4 (2025) 2402889.
[45] W. Dai, P. Wang, J. Long, et al., ACS Catal. 13 (2023) 2513–2522.
[46] L. Xiao, Q. Zheng, R. Zhou, et al., J. Energy Chem. 94 (2024) 19–28.
[47] X. Wang, B. Hu, Y. Li, Z. Yang, G. Zhang, Chin. J. Catal. 66 (2024) 257–267.
[48] B. Feng, Y. Ouyang, P. Liu, et al., Inorg. Chem. Front. 12 (2025) 6731–6739.
[49] L. Dou, H. Hu, Y. Tian, et al., Mater. Lett. 355 (2024) 135468.
[50] Z. Wang, Z. Yang, J. He, et al., Carbon Energy 7 (2025) e70032.
[51] Y. Xia, Y. Xiong, B. Lim, S..E. Skrabalak, Angew. Chem. Int. Ed. 48 (2009) 60–103.
[52] W. Huang, J. Zhu, M. Wang, et al., Adv. Funct. Mater. 31 (2021) 2007584.

[53] T. Nagao, S. Yaginuma, M. Saito, et al., Surf. Sci. 590 (2005) 247–252.
[54] P. Li, F. Yang, J. Li, et al., Adv. Energy Mater. 13 (2023) 2301597.
[55] M. Zhao, Y. Gu, W. Gao, et al., Appl. Catal. B 266 (2020) 118625.
[56] W. Zhang, Y. Hu, L. Ma, et al., Nano Energy 53 (2018) 808–816.
[57] T. Chai, X. Li, T. Feng, et al., Nanoscale 10 (2018) 17617–17622.
[58] Z. Yu, S. Wu, L. Chen, et al., ACS Appl. Mater. Interfaces 14 (2022) 10648–10655.
[59] N. Hussain, T. Liang, Q. Zhang, et al., Small 13 (2017) 1701349.
[60] F. Reis, G. Li, L.M. Bauernfeind, et al., Science 357 (2017) 287–290.
[61] A. Fang, C. Adamo, S. Jia, et al., Sci. Adv. 4 (2018) eaaq0330.
[62] J. Zhu, J. Li, R. Lu, et al., Nat. Commun. 14 (2023) 4670.
[63] X. Chen, S. Lv, H. Gu, et al., Angew. Chem. Int. Ed. 63 (2024) e202407665.
[64] X. Liang, Q. Zheng, N. Wei, et al., Nano Energy 114 (2023) 108638.
[65] M. Zhang, J. Wang, X. Rong, X. Lu, T. Lu, Nano Res. 17 (2023) 2381.
[66] H. Yang, N. Han, J. Deng, et al., Adv. Energy Mater. 8 (2018) 1801536.
[67] N. Han, Y. Wang, H. Yang, et al., Nat. Commun. 9 (2018) 1320.
[68] F.P.G. Arquer, O.S. Bushuyev, P.D. Luna, et al., Adv. Mater. 30 (2018) 1802858.
[69] C. Cao, D. Ma, J. Gu, et al., Angew. Chem. Int. Ed. 59 (2020) 15014–15020.
[70] X. Fu, J. Wang, X. Hu, et al., Adv. Funct. Mater. 32 (2021) 2107182.
[71] D. Xia, H. Yu, H. Xie, et al., Nanoscale 14 (2022) 7957–7973.
[72] F. Yang, A.O. Elnabawy, R. Schimmenti, et al., Nat. Commun. 11 (2020) 1088.
[73] L. Chen, Y. Hao, J. Li, et al., Small 34 (2023) 2301639.
[74] L. Zhao, J. Wang, R. Yan, et al., Small 2 (2025) 2406109.
[75] W. Yan, Y. Zhang, G. Dong, Y. Bi, EES Catal. 3 (2025) 268–273.
[76] Y. Bai, C. Cheng, Z. Shi, et al., ACS Appl. Nano Mater. 5 (2022) 11561–11567.
[77] M. Wang, H. Wang, Y. Gu, et al., ACS Mater. Lett. 6 (2024) 100–108.
[78] Y. Hu, J. Liang, Y. Gu, et al., Nano Lett. 23 (2023) 10512–10521.
[79] L. Xue, Y. Qi, Z. Li, et al., J. Energy Chem. 110 (2025) 88–108.
[80] L. Su, Q. Hua, Y. Yang, et al., J. Energy Chem. 105 (2025) 326–351.
[81] X. Wang, D. Song, C. Wang, et al., ACS Appl. Nano Mater. 6 (2023) 17357–17363.
[82] M. Duan, Y. Xie, H. Han, et al., Nano Res. 18 (2025) 94907448.
[83] A. He, C. Wang, N. Zhang, et al., Appl. Surf. Sci. 638 (2023) 158140.
[84] S. Liu, T. Wang, X. Liu, et al., ACS Catal. 14 (2024) 489–497.
[85] X. Yue, C. Guan, H. Yang, M. Chen, Q. Xiang, Small 21 (2025) 2412527.
[86] Y. Mao, Y. Jiang, Q. Gou, et al., Appl. Catal. B 340 (2024) 123189.
[87] Y. Li, Y. Li, X. Liang, et al., ACS Appl. Nano Mater. 5 (2022) 7019–7028.
[88] H. Wang, X. Wang, P. Hu, et al., Appl. Catal. B 351 (2024) 123956.
[89] X. Huang, X. Han, R. Tang, et al., ACS Appl. Mater. Interfaces 16 (2024) 742–751.
[90] K. Wu, P. Yang, S. Fan, et al., J. Mater. Chem. A 12 (2024) 33972–33983.
[91] N. Li, P. Yan, Y. Tang, et al., Appl. Catal. B 297 (2021) 120481.
[92] J. Xu, S. Yang, L. Ji, et al., Nano Res. 16 (2023) 53–61.
[93] L. Yi, J. Chen, P. Shao, et al., Angew. Chem. Int. Ed. 59 (2020) 20112–20119.
[94] B. Kao, Y. Zeng, Y. Lee, et al., Small 20 (2024) 2307910.
[95] N. Palanimuthu, M.R. Subramaniam, M.A.P.P.K. Sharma, et al., Small 40 (2024) 2400913.
[96] X. Chen, R. Lu, C. Li, et al., Nat. Commun. 16 (2025) 1927.
[97] X. Zhang, X. Liang, H. Yan, et al., Nano Lett. 25 (2025) 10152–10160.
[98] Z. Wang, Z. Yang, J. He, et al., ACS Nano 19 (2025) 21492–21505.
[99] S. Ruan, B. Zhang, J. Zou, et al., Chin. J. Catal. 12 (2022) 3161–3169.
[100] D. Wang, C. Liu, Y. Zhang, et al., Small 17 (2021) 2100602.
[101] Y. Hu, D. Lu, W. Zhou, X. Wang, Y. Li, J. Mater. Chem. A 11 (2023) 1937–1943.
[102] D. Wang, K. Chang, Y. Zhang, et al., Appl. Catal. B 299 (2021) 120693.
[103] B. Li, X. Liu, H. Zhu, H. Guan, R. Guo, Small 49 (2024) 2406074.
[104] Y. Wang, S. Wang, R. Li, et al., Carbon 162 (2020) 586.
[105] Q. Yu, J. Wang, H. Li, et al., Chem. Eng. J. 429 (2022) 132102.
[106] A. Xu, X. Chen, D. Wei, et al., J. Xu, Small 19 (2023) 2302253.
[107] H. Wei, A. Tan, Z. Xiang, et al., ChemSusChem 15 (2022) e202200752.
[108] L. Lv, R. Lu, J. Zhu, et al., Angew. Chem. Int. Ed. 62 (2023) e202303117.
[109] Y. Liu, T. Wu, H. Cheng, et al., Nano Res. 16 (2023) 10803–10809.
[110] X. Cao, Y. Tian, J. Ma, et al., Adv. Mater. 36 (2024) 2309648.
[111] R. Nankya, Y. Xu, A. Elgazzar, et al., Angew. Chem. Int. Ed. 63 (2024) e202403671.
[112] Z. Jiang, S. Ren, X. Cao, et al., Angew. Chem. Int. Ed. 63 (2024) e202408412.
[113] H. Zheng, G. Wu, G. Gao, X. Wang, Chem. Eng. J. 421 (2021) 129606.
[114] Z. Zhang, Z. Zhang, J. He, et al., Angew. Chem. Int. Ed. 64 (2025) e202515485.
[115] H. Zhao, Y. Xie, B. Lv, G. Jing, Y. Li, Appl. Catal. B 371 (2025) 125234.
[116] M. Zhang, W. Zhu, Z. Liu, et al., Angew. Chem. Int. Ed. 64 (2025) e202510206.
[117] L. Wang, B. Deng, H. Xie, et al., J. Energy Chem. 113 (2026) 598–609.
[118] J. Wu, Y. Li, M. Hu, et al., Angew. Chem. Int. Ed. 65 (2026) e202516163.
[119] J. Yang, X. Wang, Y. Qu, et al., Adv. Energy. Mater. 10 (2020) 2001709.
[120] Y. Xiao, D. Liu, J. Yang, et al., Nano Lett. 25 (2025) 6548–6555.
[121] Z. Li, Y. Yang, H. Ding, et al., Chem Catal. 3 (2023) 100767.
[122] G. Liu, Y. Chen, Y. Chen, et al., Adv. Mater. 35 (2023) 2304716.
[123] W. Yin, B. Liu, X. Wang, et al., Sci. China Mater. 67 (2024) 1965–1974.
[124] X. Jing, Z. Zhu, L. Chen, et al., ACS Appl. Mater. Interfaces 15 (2023) 20317–20324.
[125] S. Liu, X. Lu, J. Xiao, X. Wang, X. Lou, Angew. Chem. Int. Ed. 58 (2019) 13828–13833.
[126] L. Li, F. Cai, F. Qi, D. Ma, J. Alloy. Compd. 841 (2020) 155789.
[127] R. Chen, J. Zhao, X. Zhang, et al., J. Am. Chem. Soc. 146 (2024) 24368–24376.
[128] Y. Yuan, Q. Wang, Y. Qiao, et al., Adv. Energy Mater. 12 (2022) 2200970.
[129] Q. Huang, X. Sha, R. Yang, H. Li, J. Peng, ACS Appl. Mater. Interfaces 16 (2024) 13882–13892.
[130] D. Yao, C. Tang, A. Vasileff, et al., Angew. Chem. Int. Ed. 60 (2021) 18178–18184.
[131] H. Liu, Y. Bai, M. Wu, et al., Angew. Chem. Int. Ed. 63 (2024) e202411575.
[132] Y. Jiang, Q. Chen, D. Wang, et al., Nano Res. 16 (2023) 6661–6669.
[133] N.B.D. Monti, T. Chen, L. Huang, et al., Chem. Lett. 16 (2025) 3761–3768.
[134] K. Yang, M. Li, T. Gao, et al., Nat. Commun. 15 (2024) 7060.